Computers and Geotechnics 129 (2021) 103862

Contents lists available at ScienceDirect

Computers and Geotechnics

journal homepage: www.elsevier.com/locate/compgeo

Research Paper

A vertical and radial consolidation analysis incorporating drain degradation based on the spectral method

Bin-Hua Xu [a,b,c,d], Buddhima Indraratna [e,*], Thanh Trung Nguyen [f], Rohan Walker [g]

[a] Geotechnical Engineering Department, Key Laboratory of Failure Mechanism and Safety Control Techniques of Earth-rock Dam of the Ministry of Water Resources, Nanjing Hydraulic Research Institute, Nanjing, China
[b] College of Civil and Transportation Engineering, Hohai University, Nanjing, China
[c] State Key Laboratory of Hydrology-Water Resources and Hydraulic Engineering, Nanjing Hydraulic Research Institute, Nanjing, China
[d] Transport Research Centre, School of Civil and Environmental Engineering, University of Technology Sydney, Broadway, Sydney, NSW 2007, Australia
[e] Distinguished Professor of Civil Engineering, and Director, Transport Research Centre, School of Civil and Environmental Engineering, University of Technology Sydney, Broadway, Sydney, NSW 2007, Australia
[f] Research Fellow, Transport Research Centre, School of Civil and Environmental Engineering, University of Technology Sydney, Broadway, Sydney, NSW 2007, Australia
[g] Geotechnical Team Leader at Maxwell GeoSystems, Research Associate, University of Wollongong, Wollongong City, NSW 2522, Australia

ARTICLE INFO

Keywords:
Spectral method
Radial consolidation
Drain degradation
Multi-layered soil
Discharge capacity

ABSTRACT

The use of prefabricated vertical drains (PVDs) to improve soft soil has received much attention in the recent past, however, there is still a lack of rigorous analytical solutions that can incorporate the time- and depth-dependent behaviour of drains into the consolidation of multi-layered soil. This study thus presents a novel approach where the spectral method is used to capture the degradation in discharge capacity of drains over time and depth, while the average consolidation of different soil layers with regard to vertical and radial drainage is computed. In this approach, the excess pore water pressure profile across different soil layers is described as a single expression using matrix operations. This proposed method is then verified with laboratory and field investigations where the degradation of PVDs is captured and compared with other solutions. The results show that this method can predict the soil behaviour with greater accuracy and flexibility whereas there is a significant deviation in the predicted consolidation when the degradation of drains is not considered properly. A parametric investigation is also carried out using the proposed solution to further highlight its ability to evaluate the effect that drain degradation can have on the consolidation of multi-layered soil.

1. Introduction

Prefabricated vertical drains (PVD) are widely used to accelerate the consolidation of soft soils (Chai et al. 2020; Feng et al. 2017; Indraratna et al. 2004, 2016, 2018; Nguyen et al. 2018b; Tang and Onitsuka 2001). Based on some specific assumptions, many analytical solutions have been proposed for the consolidation of homogeneous soil induced by vertical drains (Barron 1948; Chai et al. 2001; Hansbo 1981, 2001; Indraratna et al. 2005, 2007; Tang and Onitsuka 2000), but since the sedimentary history and stress conditions differ, most soft soils are rarely homogeneous and usually consist of several different layers (Liu et al. 2014; Walker and Indraratna 2009). Therefore, many solutions for multi-layered soil consolidation induced by vertical drains have been developed, for example Tang and Onitsuka (2001), and Tang et al. (2013) presented an analytical solution for soil consolidation considering specific 2 and 3 layers. Nogami and Li (2003) used the transfer matrix method to calculate the consolidation of clay soil with a system of thin horizontal drains and vertical cylindrical drains, however, these can only consider two to three layers, which is not flexible enough for soil with more complex stratification. Moreover, the change of total stress with time and depth is usually ignored, which makes it difficult to capture the behaviour of soil over depth with any degree of accuracy.

Some later studies attempted to solve the consolidation of multi-layered soil considering the distribution of stress over time and depth. Liu et al. (2014) for example, presented a quasi-analytical method to solve the equal strain consolidation of multi-layered soil with a vertical drain system. Zhou et al. (2017) proposed an analytical solution for a multi-layered soil system under a surcharge combined with PVD and vacuum preloading, while simplifying the explicit expressions for one and two-layer systems. However, their models become complex when

* Corresponding author.
E-mail address: buddhima.indraratna@uts.edu.au (B. Indraratna).

https://doi.org/10.1016/j.compgeo.2020.103862
Received 17 June 2020; Received in revised form 22 September 2020; Accepted 24 September 2020
Available online 2 November 2020

involving separate governing equations with unknown coefficients in each layer. Furthermore, many approaches will not be able to derive closed-form solutions when the soil parameters vary with time and depth. This cumbersome implementation and limited loading choices render these methods fundamentally impractical and thus limit their application in large field projects.

Walker et al. (2009) and Walker and Indraratna (2009) applied, for the first time, a powerful variation of the spectral method to solve the governing consolidation equations of multi-layered soil considering both vertical and radial drainage. Subsequently, Walker and Indraratna (2015) further developed this technique by incorporating the varying permeability of drains with depth. Unlike conventional numerical methods such as finite element method (FEM) and finite difference method (FDM), spectral methods use global basis functions that can accelerate computational accuracy and memory optimization (Boyd 2000; Trefethen 2000). Despite this advancement, previous studies have not fully incorporated the time- and depth-dependent discharge capacity of drains into the overall consolidation behaviour of soil well.

Physical factors such as clogging due to fine silt intrusion, large strain deformation, the potential kinking and bending (Deng et al. 2013a; 2013b, 2014; Kim et al. 2018; Tran-Nguyen et al. 2010; Xu et al. 2020), and bio-chemical factors such as bacterial activity, high organic and acidic environment (Indraratna et al. 2016; Kim and Cho 2008; Nguyen et al. 2018a, 2018b) can cause a considerable reduction in the discharge capacity of drains with time. For instance, Chai and Miura (1999), Kim and Cho (2008), Kim et al. (2011), Bo et al. (2016) and Nguyen et al. (2018a) investigated the retarded capacity discharge of PVDs over time by laboratory tests, while some other field data (Bergado et al. 1996) showed considerable retardation of the consolidation curves at deeper layers, where the discharge capacity of drains has decreased. Moreover, a reduced discharge capacity is often more apparent in relatively long drains (Deng et al. 2013a, 2013b; Indraratna et al. 2016; Kim et al. 2018; Nguyen and Kim 2019). For example, in a typical 20 m deep soil treated by PVDs with a strain >7.5%, 1.5–2.0 m of settlement will probably cause considerable bending and/or kinking, and thus reduce the discharge capacity of the PVDs. Note also that in the current study, the term degradation is used to represent both physical (i.e., clogging, bending and kinking) and biodegradable processes that weaken the engineering properties (i.e., reduced discharge capacity) of drains.

Although a lot of effort has gone into evaluating how the drain degradation affects the consolidation of soil in recent years (Deng et al. 2013a, 2013b; Indraratna et al. 2016; Nguyen et al. 2018b; Nguyen and Kim 2019), but since they consider the soil to be homogeneous so they cannot incorporate multi-layered soil very well. In addition, most of these previous formulae are only proposed for radial consolidation, so Carrillo's law is later needed to calculate the total degree of consolidation, which actually does not capture well the simultaneous contribution of different drainages to the overall consolidation of soil in the field. Therefore, a more complete vertical and radial consolidation analysis that incorporates drain degradation for multi-layered soils to predict total consolidation becomes essential.

This paper aims to improve the original solution of Walker and Indraratna (2015) by considering the retardation of drain efficiency with both time and depth, so that a more realistic and rigorous theoretical solution for the PVD-assisted soil consolidation can be achieved. The spectral method is used to solve governing equations based on common matrix operations and the different distribution patterns of soil parameters and loading forms are taken into account. The excess pore water pressure (EPWP) and settlement profiles across different soil layers are given by the matrix expressions as the key advantages enjoyed by the current spectral method approach. The proposed model is then verified against experimental and field data, and also compared with previous solutions to further highlight the advanced features of this model. The effects that different rates of drain degradation and initiations can have on the consolidation of multi-layer soil are also discussed.

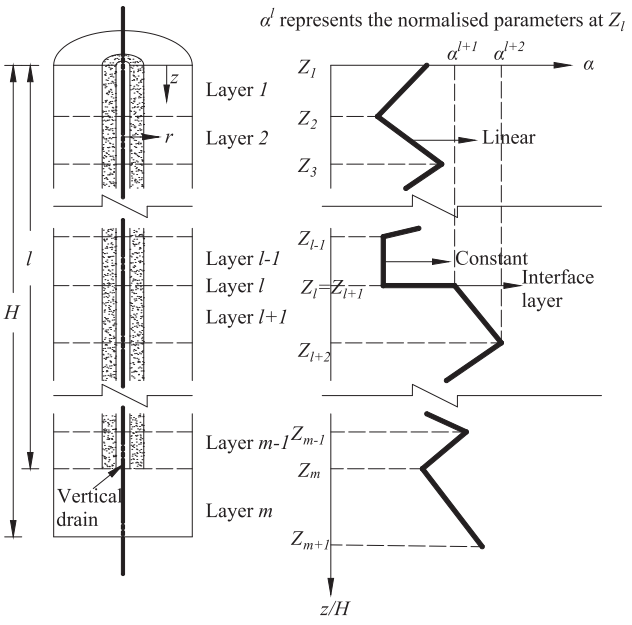

Fig. 1. . Soil and drain properties of multi-layered soil.

2. Mathematical formulation

2.1. Overall governing equation of soil consolidation

Given a stratified soil with a vertical drain (Fig. 1), the governing partial differential equation for soil consolidation, while considering vertical and radial drainage with depth-dependent soil properties, can be given by (Walker and Indraratna 2015):

$$\frac{m_v}{\overline{m}_v}\frac{\partial \overline{u}}{\partial t} = -dT_h\frac{\eta}{\overline{\eta}}\overline{u} + dT_v\frac{\partial}{\partial Z}\left(\frac{k_v}{\overline{k}_v}\frac{\partial \overline{u}}{\partial Z}\right) + \frac{m_v}{\overline{m}_v}\frac{\partial \overline{\sigma}}{\partial t} + dT_h\frac{\eta}{\overline{\eta}}u_w \tag{1}$$

$$dT_h\frac{\eta}{\overline{\eta}}u_w - dT_w\frac{\partial}{\partial Z}\left(q_w\frac{\partial u_w}{\partial Z}\right) = dT_h\frac{\eta}{\overline{\eta}}\overline{u} \tag{2}$$

where

$$Z = \frac{z}{H},\quad \eta = \frac{k_h}{\mu r_e^2},\quad dT_v = \frac{\frac{\overline{k}_v}{\gamma_w \overline{m}_v H^2}}{dT_h = \frac{2\overline{\eta}}{\gamma_w \overline{m}_v}},\quad dT_w = \frac{1}{\gamma_w \overline{m}_v H^2 (n^2-1)\pi r_w^2}$$

In the above, $\overline{u}$ is the average EPWP at a particular depth, u_w is the prescribed pore pressure in the drain, $\overline{\sigma}$ is the average total stress at a particular depth, t is the time, z is the depth, H is the total depth of soil, γ_w is the unit weight of water, m_v is the coefficient of volume compressibility, k_v is the vertical permeability, k_h is the undisturbed horizontal permeability,q_w is the drain discharge capacity, r_w is the radius of the drain, r_e is the radius of influence zone, n is the ratio between $r_e$and r_w. $\overline{k}_v$, $\overline{m}_v$, and $\overline{\eta}$ are convenient reference values for the relevant parameters. μ is the dimensionless drain parameter, which is related to the smear zone and radial geometry of the drain (Walker and Indraratna 2015). Note that in this approach Eqs. (1) and (2) depicts the dissipation of EPWP in the soil and drain domains individually.

2.2. Analytical solution of governing equation with the spectral method

For the spectral method, the EPWP $\overline{u}(Z,t)$ and the prescribed pore pressure in the drain u_w are expressed as a truncated series of N terms, which in matrix form is:

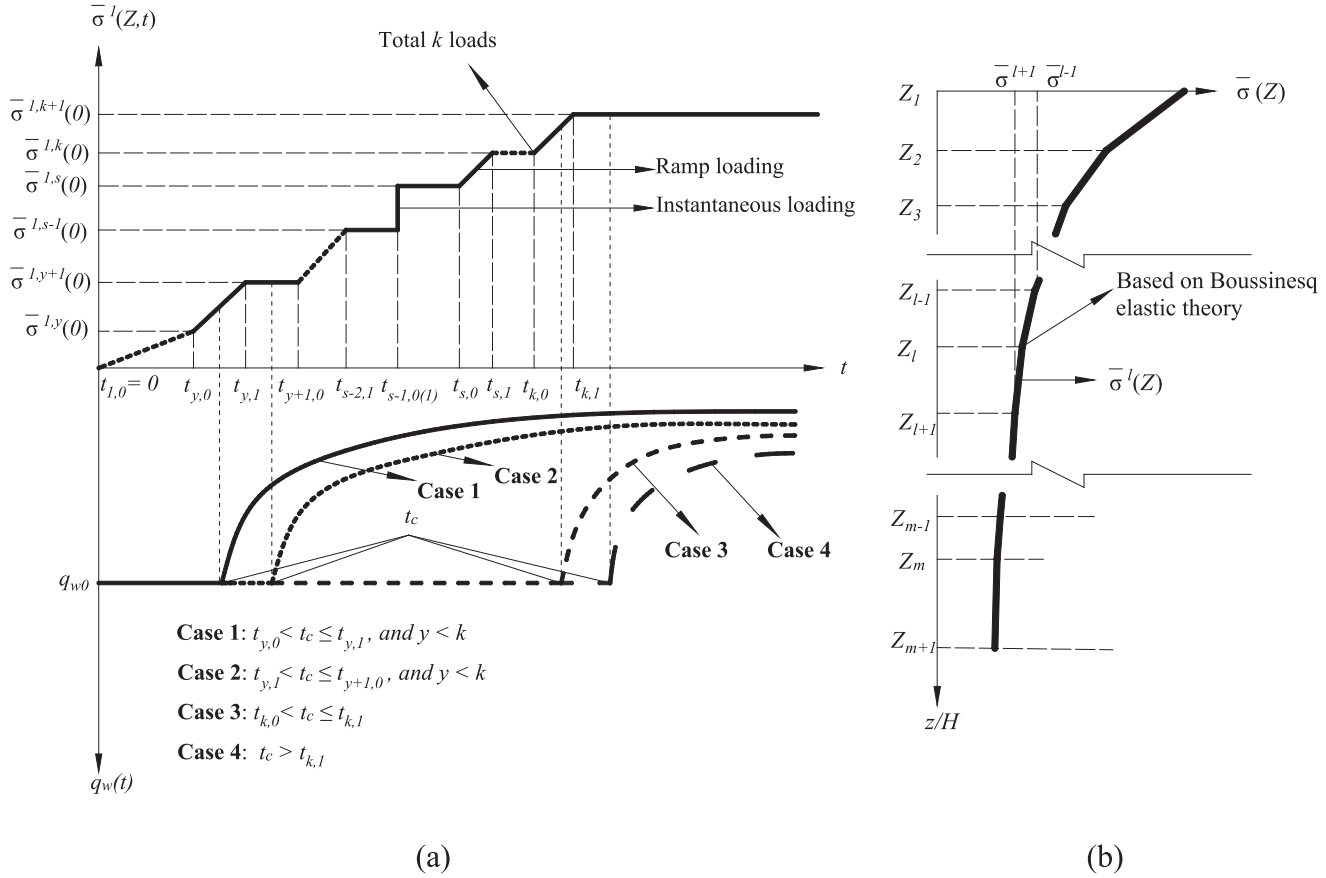

Fig. 2. . Distribution models for loading and stress: (a) multi-ramp loading process and t_c location; (b) stress distribution over the depth of multi-layered soil.

$$\overline{u}(Z,t) \approx \sum_{j=1}^{N} \phi_j(Z) A_j(t) = \boldsymbol{\phi A} \tag{3}$$

$$u_w(Z,t) \approx \sum_{j=1}^{N} \phi_j(Z) B_j(t) = \boldsymbol{\phi B} \tag{4}$$

where

$$\boldsymbol{\phi} = [\,\phi_1(Z) \quad \phi_2(Z) \quad \cdots. \quad \phi_N(Z)\,] \tag{5}$$

$$\boldsymbol{A}^T = [\,A_1(t) \quad A_2(t) \quad \cdots. \quad A_N(t)\,] \tag{6}$$

$$\boldsymbol{B}^T = [\,B_1(t) \quad B_2(t) \quad \cdots. \quad B_N(t)\,] \tag{7}$$

In the matrix $\boldsymbol{\phi}$, $\phi_j(Z)$ is a set of independent basis functions, and in matrix $\boldsymbol{A}$ and$\boldsymbol{B}$, $A_j(t)$ and $B_j(t)$ are expansion coefficients which can be determined by the operator, they involve governing partial differential equations that can vary with time. The basis functions are chosen to satisfy the boundary conditions of governing equation (Boyd 2000). For pervious top and pervious bottom (PTPB) conditions $\overline{u}(0,t) = 0$ and $\overline{u}(H, t) = 0$, and for pervious top and impervious bottom (PTIB) conditions $\overline{u}(0,t) = 0$ and $\partial\overline{u}(H,t)/\partial z = 0$. Thus, the suitable basis function is:

$$\phi_j(Z) = \sin(M_j Z) \tag{8}$$

where

$$M_j = \begin{cases} j\pi & for\ PTPB \\ \dfrac{\pi}{2}(2j-1) & for\ PTIB \end{cases} \tag{9}$$

The test functions for the spectral Galerkin method are the same as the basis ones. By combining Eqs. (1) and (2), and then using the weighted residual method and the initial condition $\boldsymbol{A}(0) = 0$, the expression of EPWP at any depth and time can be obtained in matrix notation as follows (see **Appendix A.1** for derivation):

$$\overline{u}(Z,t) = \boldsymbol{\phi} e^{-\int_0^t \boldsymbol{\Gamma}^{-1}\left(\boldsymbol{\psi}+\boldsymbol{\zeta}-\boldsymbol{\psi}(\boldsymbol{\psi}+\boldsymbol{\chi})^{-1}\boldsymbol{\psi}\right)d\tau} \int_0^t e^{\int_0^\tau \boldsymbol{\Gamma}^{-1}\left(\boldsymbol{\psi}+\boldsymbol{\zeta}-\boldsymbol{\psi}(\boldsymbol{\psi}+\boldsymbol{\chi})^{-1}\boldsymbol{\psi}\right)dt} \boldsymbol{\Gamma}^{-1}\boldsymbol{\theta} d\tau \tag{10}$$

where the elements of matrices $\boldsymbol{\Gamma}$, $\boldsymbol{\psi}$ and $\boldsymbol{\zeta}$ are determined by the distribution of m_v, η and k_v, respectively, which are depth-dependent. The elements of matrix $\boldsymbol{\chi}$ are determined by the distribution of q_w, which varies with depth and time. The elements of matrix $\boldsymbol{\theta}$ are determined by the combined distribution of m_v and $\partial\overline{\sigma}/\partial t$ (see Eqs. (28)-(32) in **Appendix A.1**).

In this paper, Z_l and Z_{l+1} denote the normalised depth at the top and bottom of the l^{th} layer, respectively. The concise expressions of parameters are used to better establish the relationship between the material parameters and each layer of soil. m_v^l, k_v^l, η^l, k_h^l and $\overline{\sigma}^l$ are used to represent the values of $\frac{m_v}{\overline{m}_v}$, $\frac{k_v}{\overline{k}_v}$, $\frac{\eta}{\overline{\eta}}$, k_h and $\overline{\sigma}$ at the normalised depth Z_l. For simplicity, α is defined to represent the normalised parameters, andα^l represents the normalised parameters at a normalised depth Z_l. Note that these values vary linearly within the layer from its top to bottom where the values m_v^{l+1}, k_v^{l+1}, η^{l+1}, $k_h^{l+1}$and $\overline{\sigma}^{l+1}$of the next layer, i.e., $l+1$th layer are considered (see Fig. 1).

Since the EPWP at each depth is expressed as a function related to depth and time, the average pore water pressure and settlement at any time can be obtained by a certain relationship. The average pore water pressure $\overline{u}_{avg}(Z_l, Z_{l+1}, t)$ and settlement $S(Z_l, Z_{l+1}, t)$ in the l^{th} layer (between depths Z_l and Z_{l+1}) can be calculated, respectively by:

$$\overline{u}_{avg}(Z_l, Z_{l+1}, t) = \frac{1}{Z_{l+1} - Z_l}\left(\int_{Z_l}^{Z_{l+1}} \boldsymbol{\phi} dZ\right)\boldsymbol{A}(t) \tag{11}$$

$$S(Z_l, Z_{l+1}, t) = H \int_{Z_l}^{Z_{l+1}} m_v(Z)(\overline{\sigma}(Z,t) - \overline{u}(Z,t))dZ \tag{12}$$

The integrals in the above equations are based on certain assumptions (see below), and their explicit matrix forms are discussed later in section 3 and **Appendix A**.

2.3. Assumptions

In this study, the following assumptions were considered while developing the model.

(1) Soil parameters such as m_v, k_v, η andk_h are assumed to be linearly distributed in each layer, and which can be represented as a linear function of Z for each certain l^{th} layer of soil (independent of time), as shown in Fig. 1, noting that the parameters in Eq. (1) are not written in explicit form as $\alpha^l(Z)$.
(2) The compressibility m_v and the vertical permeability coefficient k_v in the smear and undisturbed zones are assumed to be equal.
(3) The total vertical stress is assumed to be the same in the radial direction at the same depth while its value at the upper and lower interface of the certain l^{th} layer is based on Boussinesq elastic theory, and the value within such a layer is assumed to be linearly distributed (Fig. 2).
(4) The velocity of pore water flow is governed by Darcy's law, and in order to include flow in the vertical direction it is assumed that this flow in the vertical direction is based on the average EPWP gradient, following the approach of Tang and Onitsuka (2000) and Wang and Jiao (2004).
(5) Pore water flows in both vertical and horizontal directions, whereas strain only occurs in the vertical direction, these strains are equal in the radial direction (equal strain).

3. Depth and time-dependent parameters and corresponding solutions

3.1. Mathematical expression for the varying q_w

For simplicity, conventional studies usually assume that q_w is a constant. In the solution of Walker and Indraratna (2015), the discharge capacity q_w could vary linearly with depth, but it assumed that drain permeability remained constant over time. Some recent studies have shown that the exponential form can be used to reasonably represent the discharge capacity degradation of drains over time (Deng et al. 2013b; Indraratna et al. 2016; Nguyen and Kim 2019; Nguyen and Indraratna 2016). In the current study, therefore, the discharge capacity q_w of drains is described as a function of time and depth, which is linearly related to depth Z for each certain l^{th} layer and exponentially related to time t. q_w^l is used to represent the value of discharge capacity q_w in the l^{th} layer. Mathematically, the discharge capacity within the depth of the l^{th} layer can be written explicitly as:

$$q_w^l = q_w^l(Z,t) = \begin{cases} q_{w0}^l + \dfrac{q_{w0}^{l+1} - q_{w0}^l}{Z_{l+1} - Z_l}(Z - Z_l) & t \le t_c \\ \left(q_{w0}^l + \dfrac{q_{w0}^{l+1} - q_{w0}^l}{Z_{l+1} - Z_l}(Z - Z_l)\right) e^{-\omega(t-t_c)} & t > t_c \end{cases} \tag{13}$$

Define $Q_w^l(Z) = q_{w0}^l + \frac{q_{w0}^{l+1} - q_{w0}^l}{Z_{l+1} - Z_l}(Z - Z_l)$ and $Q_w(t) = \begin{cases} 1 & t \le t_c \\ e^{-\omega(t-t_c)} & t > t_c \end{cases}$. The function of the discharge capacity in the l^{th} layer becomes $q_w^l(Z,t) = Q_w^l(Z)Q_w(t)$. In the above, q_{w0}^l is the initial discharge capacity at the normalised depth Z_l (at the top of the l^{th} layer), q_{w0}^{l+1} is the initial discharge capacity at the normalised depth Z_{l+1} (at the bottom of the l^{th} layer), t_c is the start time of degradation, ω (with dimension of $1/T$) is the decay coefficient that represents the rate of degradation in q_w with time.

In this study, it is assumed that the discharge capacity in each layer starts to degrade with the same degradation rate at the same time, and it should be required that $\omega \ge 0$. Note that when $q_{w0}^{l+1} = q_{w0}^l$, the discharge capacity does not vary with depth in the l^{th} layer; and when the degradation has not taken place, i.e., $t < t_c$, q_w is only a function with depth.

3.2. Expressions for parameters varying with depth and time

Based on assumption (1), soil parameters such as m_v^l, k_v^l, η^l and k_h^l are described as a linear functions of Z in each certain l^{th} layer of soil, which can be written explicitly as $\alpha^l(Z) = \alpha^l + \frac{\alpha^{l+1} - \alpha^l}{Z_{l+1} - Z_l}(Z - Z_l)$. Note that if $\alpha^l = \alpha^{l+1}$, the corresponding soil parameter is constant in the considered layer, but if the parameter has a mutation at a certain depth, then the concept of an interface layer is proposed, the thickness of the interface layer is 0 ($Z_l = Z_{l+1}$), as shown in Fig. 1. Following assumption (3), the value of vertical stress $\overline{\sigma}^l$ at a normalised depth Z_l is calculated by Boussinesq elastic theory, while the distribution of total stress in the certain l^{th} layer of soil $\overline{\sigma}^l(Z)$ is assumed to vary with both depth and time. To obtain an explicit analytical solution, a single equation describing the distribution of total stress in the certain l^{th} layer of soil is given by:

$$\overline{\sigma}^l(Z,t) = \sum_{s=1}^{k} F_s(t)\left(\overline{\sigma}^{l,s+1}(Z) - \overline{\sigma}^{l,s}(Z)\right) \tag{14}$$

where

$$\overline{\sigma}^{l,s}(Z) = \overline{\sigma}^{l,s} + \frac{\overline{\sigma}^{l+1,s} - \overline{\sigma}^{l,s}}{Z_{l+1} - Z_l}(Z - Z_l) \tag{15}$$

$$F_s(t) = \begin{cases} \dfrac{t - t_{s,0}}{t_{s,1} - t_{s,0}} H\langle t - t_{s,0}\rangle\left(1 - H\langle t - t_{s,1}\rangle\right) + H\langle t - t_{s,1}\rangle & \text{for } t_{s,0} < t_{s,1} \\ H\langle t - t_{s,1}\rangle & \text{for } t_{s,0} = t_{s,1} \end{cases} \tag{16}$$

where depth Z belongs to the l^{th} layer of soil, $\overline{\sigma}^{l,s+1}(Z)$ is the total stress at depth Z in the l^{th} layer of soil at the beginning time of the $s+1$th (or the end time of the s^{th}) loading (ramp or instantaneous), $H\langle t - t_{i,j}\rangle$ is the Heaviside step function, k is the total number of loading, $t_{s,0}$ and $t_{s,1}$ are the start time and end time of the s^{th} loading (ramp or instantaneous), respectively, as shown in Fig. 2**(a)**. Note that if $t_{s,0} = t_{s,1}$, the load is instantaneous loading; if $t_{s,0} < t_{s,1}$, that means the load is ramp loading.

3.3. Corresponding solutions

According to the previous section 2.2, $\boldsymbol{\chi}$ is a matrix function related to time t when considering the time-dependent discharge capacity; the elements of matrix $\boldsymbol{\theta}$ are related to $\partial\overline{\sigma}/\partial t$, and $\boldsymbol{\theta}$ is also a matrix function related to time t when considering the time-dependent surcharge. In the s^{th} loading, $\boldsymbol{\theta}$ can be expressed by $\boldsymbol{\theta}(s) = F_s^{'}(t)\boldsymbol{\Theta}(s)$ where $\boldsymbol{\Theta}(s)$ is a matrix independent of time (see Eqs. (60) and (63) in **Appendix A.2**). Combined with Eq. (16), $F_s^{'}(t)$ can be calculated by:

$$F_s^{'}(t) = \begin{cases} \dfrac{1}{t_{s,1} - t_{s,0}} & \text{for } t_{s,0} < t_{s,1} \quad (\textit{ramp loading}) \\ \delta(t - t_{s,1}) & \text{for } t_{s,0} = t_{s,1} \quad (\textit{instantaneous loading}) \end{cases} \tag{17}$$

where $\delta(x)$ is the Dirac delta function.

When $t \le t_c$, $Q_w(t)$ is a constant value, which is equal to 1. So the matrix $\boldsymbol{\chi}$ is a constant matrix, which is the same as $\boldsymbol{X}$ (as shown in Eqs. (53)-(55)). Define $\boldsymbol{G} = \boldsymbol{\Gamma}^{-1}(\boldsymbol{\psi} + \boldsymbol{\zeta})$ and $\boldsymbol{M} = \boldsymbol{\Gamma}^{-1}\left(\boldsymbol{\psi}(\boldsymbol{\psi} + \boldsymbol{X})^{-1}\boldsymbol{\psi}\right)$, then the integration $\int_0^t \boldsymbol{\Gamma}^{-1}\left(\boldsymbol{\psi} + \boldsymbol{\zeta} - \boldsymbol{\psi}(\boldsymbol{\psi} + \boldsymbol{\chi})^{-1}\boldsymbol{\psi}\right)d\tau$ can be calculated by:

$$\int_0^t \boldsymbol{\Gamma}^{-1}\left(\boldsymbol{\psi} + \boldsymbol{\zeta} - \boldsymbol{\psi}(\boldsymbol{\psi} + \boldsymbol{\chi})^{-1}\boldsymbol{\psi}\right)d\tau = (\boldsymbol{G} - \boldsymbol{M})t \tag{18}$$

The integration $\boldsymbol{R}(s) = \int_{t_1^s}^{t_2^s} e^{\int_0^t \boldsymbol{\Gamma}^{-1}\left(\boldsymbol{\psi}+\boldsymbol{\zeta}-\boldsymbol{\psi}(\boldsymbol{\psi}+\boldsymbol{\chi})^{-1}\boldsymbol{\psi}\right)d\tau} \boldsymbol{\Gamma}^{-1}\boldsymbol{\theta}(s)d\tau$ can be calculated by:

$$\boldsymbol{R}(s) = \begin{cases} \dfrac{1}{t_{s,1}-t_{s,0}} \dfrac{e^{(\boldsymbol{G}-\boldsymbol{M})t_2^s} - e^{(\boldsymbol{G}-\boldsymbol{M})t_1^s}}{\boldsymbol{G}-\boldsymbol{M}} \boldsymbol{\Gamma}^{-1}\Theta(s) & \textit{for ramp loading} \\ e^{(\boldsymbol{G}-\boldsymbol{M})t_{s,0}} \boldsymbol{\Gamma}^{-1}\Theta(s) H\langle t-t_{s,0}\rangle & \textit{for instantaneous loading} \end{cases} \tag{19}$$

where t_1^s,t_2^s is the integral boundary of the s^{th} loading defined by: $t_1^s = \min(t, t_{s,0})$, $t_2^s = \min(t, t_{s,1})$.

In this case, the calculation of $\boldsymbol{A}(t)$ can be described as:

$$\boldsymbol{A}(t) = e^{-(\boldsymbol{G}-\boldsymbol{M})t}\left(\sum_{s=1}^{K}(\boldsymbol{R}(s))\right) \tag{20}$$

When $t > t_c$, $\boldsymbol{\chi}$ is a matrix function related to time t. Define the integration $\boldsymbol{\Xi}(t) = \boldsymbol{\Gamma}^{-1}\int_{t_c}^{t}\boldsymbol{\psi}(\boldsymbol{\psi}+\boldsymbol{\chi})^{-1}\boldsymbol{\psi}d\tau$, and its calculation can be obtained from Eq. (65) in **Appendix A.2**. In this case, the integration $\int_0^t \boldsymbol{\Gamma}^{-1}\left(\boldsymbol{\psi}+\boldsymbol{\zeta}-\boldsymbol{\psi}(\boldsymbol{\psi}+\boldsymbol{\chi})^{-1}\boldsymbol{\psi}\right)d\tau$ can be calculated by:

$$\int_0^t \boldsymbol{\Gamma}^{-1}\left(\boldsymbol{\psi}+\boldsymbol{\zeta}-\boldsymbol{\psi}(\boldsymbol{\psi}+\boldsymbol{\chi})^{-1}\boldsymbol{\psi}\right)d\tau = \boldsymbol{G}t - \boldsymbol{M}t_c - \boldsymbol{\Xi}(t) \tag{21}$$

When $t > t_c$, calculating $\boldsymbol{A}(t)$ depends on the value of t_c so it is much more complicated. There are four cases, as shown in Fig. 2**(a)**, and the expression of $\boldsymbol{A}(t)$ is different in each case as represented specifically as follows.

Case 1:. *For $t_{y,0} < t_c \le t_{y,1}$, and $y < k$, drain degradation occurs before the loading process ends and in the y^{th} loading process, as shown in* Fig. 2**(a)**, *where $\boldsymbol{A}(t)$ can be described as*:

$$\boldsymbol{A}(t) = e^{-(\boldsymbol{G}t-\boldsymbol{M}t_c-\boldsymbol{\Xi}(t))}\left(\sum_{s=1}^{y-1}(\boldsymbol{R}(s)) + \frac{e^{(\boldsymbol{G}-\boldsymbol{M})t_c} - e^{(\boldsymbol{G}-\boldsymbol{M})t_{y,0}}}{\boldsymbol{G}-\boldsymbol{M}}\boldsymbol{\Gamma}^{-1}\boldsymbol{\theta}(y) + \int_{t_c}^{t_2^y} e^{(\boldsymbol{G}\tau-\boldsymbol{M}t_c-\boldsymbol{\Xi}(t))}d\tau\boldsymbol{\Gamma}^{-1}\boldsymbol{\theta}(y) + \sum_{s=y+1}^{k}\left(\int_{t_1^s}^{t_2^s} e^{(\boldsymbol{G}\tau-\boldsymbol{M}t_c-\boldsymbol{\Xi}(t))}\boldsymbol{\Gamma}^{-1}\boldsymbol{\theta}(s)d\tau\right)\right) \tag{22}$$

Case 2:. *For $t_{y,1} < t_c \le t_{y+1,0}$, and $y < k$, drain degradation starts between the end time of y^{th} loading and the start time of $y+1$th loading, as shown in* Fig. 2**(a)**, *where $\boldsymbol{A}(t)$ can be described as*:

$$\boldsymbol{A}(t) = e^{-(\boldsymbol{G}t-\boldsymbol{M}t_c-\boldsymbol{\Xi}(t))}\left(\sum_{s=1}^{y}(\boldsymbol{R}(s)) + \sum_{s=y+1}^{k}\left(\int_{t_1^s}^{t_2^s} e^{(\boldsymbol{G}\tau-\boldsymbol{M}t_c-\boldsymbol{\Xi}(t))}\boldsymbol{\Gamma}^{-1}\boldsymbol{\theta}(s)d\tau\right)\right) \tag{23}$$

Case 3:. *For $t_{k,0} < t_c \le t_{k,1}$, the drain starts to decay at the last loading stage, as shown in* Fig. 2**(a)**, *where $\boldsymbol{A}(t)$ can be described as*:

$$\boldsymbol{A}(t) = e^{-(\boldsymbol{G}t-\boldsymbol{M}t_c-\boldsymbol{\Xi}(t))}\left(\sum_{s=1}^{k-1}(\boldsymbol{R}(s)) + \frac{e^{(\boldsymbol{G}-\boldsymbol{M})t_c} - e^{(\boldsymbol{G}-\boldsymbol{M})t_{k,0}}}{\boldsymbol{G}-\boldsymbol{M}}\boldsymbol{\Gamma}^{-1}\boldsymbol{\theta}(k) + \int_{t_c}^{t_2^k} e^{(\boldsymbol{G}\tau-\boldsymbol{M}t_c-\boldsymbol{\Xi}(t))}\boldsymbol{\Gamma}^{-1}\boldsymbol{\theta}(k)d\tau\right) \tag{24}$$

Case 4:. *For $t_c > t_{k,1}$, the drain starts to decay after the loading process, as shown in* Fig. 2**(a)**, *where $\boldsymbol{A}(t)$ can be described as*:

$$\boldsymbol{A}(t) = e^{-(\boldsymbol{G}t-\boldsymbol{M}t_c-\boldsymbol{\Xi}(t))}\left(\sum_{s=1}^{k}\boldsymbol{R}(s)\right) \tag{25}$$

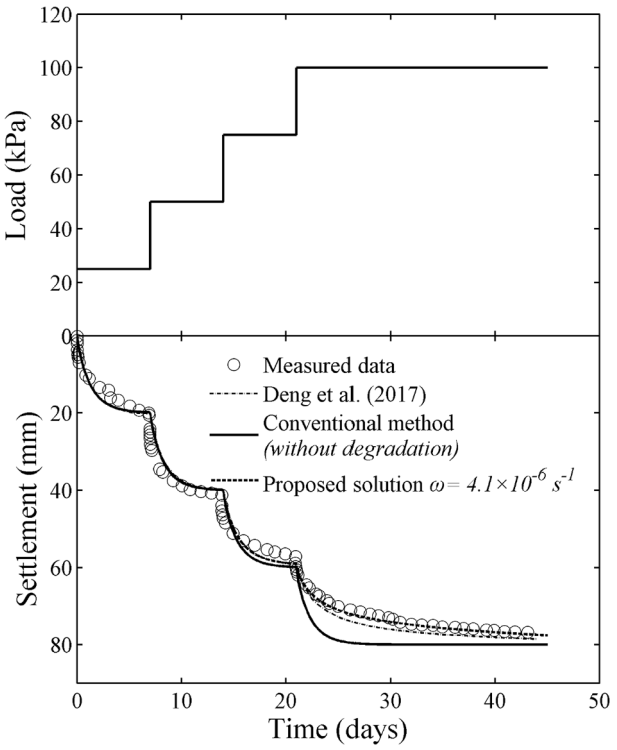

Fig. 3. . Loading process (after Deng et al. (2017)) and settlement of model test.

Note that because the integrations $\int_a^b e^{(\boldsymbol{G}t-\boldsymbol{M}t_c-\boldsymbol{\Xi})}d\tau$ in the Eqs. (22)-(24) cannot be solved analytically, a numerical approach, i.e., Simpson's rule (Barron 1948; Deng et al. 2013a) is adopted.

Loading process time in the field is relatively short compared to the time of complete consolidation, while there is little change in the deformation and stress state of the PVDs during the loading process. In reality, the exact time when a drain begins to degrade is difficult to determine in the field, so for simplicity, it can be assumed that the decay occurs after the loading process has been completed. In this way, $\boldsymbol{A}(t)$ can get an exact solution, as shown in Eq. (25), especially for the case of ramp loading.

The specific expressions for average pore water pressure $\overline{u}_{avg}(Z_l, Z_{l+1}, t)$ and settlement $S(Z_l, Z_{l+1}, t)$ between depths Z_l and Z_{l+1} are shown in Eqs. (66)-(67) in **Appendix A.2**.

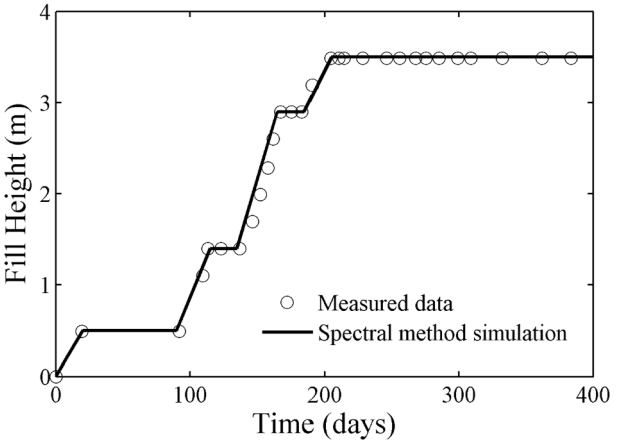

Fig. 4. . Loading process of Saga Airport test embankment (after (Chai and Miura 1999)).

Table 1
. Soil parameters for Saga Airport test embankment.

Layer	Depth (m)	λ	κ	ν	e_0	γ (kN/m^3)	k_v (10^{-8} m/s)	k_h (10^{-8} m/s)	Young's modulus, E (kPa)
B	0–1	0.25	0.025	0.25	2.00	15.0	7.60	11.40	—
Ac1	1–4	0.44	0.044	0.30	2.00	14.5	3.80	5.70	—
As1	4–5.6	—	—	0.20	—	15.5	290	290	10,000
Ac2	5.6–21	0.87	0.087	0.30	2.50	14.5	1.76	2.64	—
As2	21–23.7	—	—	0.20	—	16.0	290	290	15,000
Ac3	23.7–25	0.30	0.030	0.30	1.75	16.0	1.76	2.64	—

4. Verification of the model

To verify this proposed model, the mathematical formulation presented above is applied to previous laboratory and field studies where the influence of drain degradation on soil consolidation is represented. The following studies are adopted.

1. Vertical and radial consolidation of single layer by multi-instantaneous loading (Deng et al. 2017)
2. Vertical and radial consolidation of multi-layered soil by multi-ramp loading (Bergado et al. 1996, Chai and Miura 1999, Deng et al. 2014);

In these two cases, the calculation of the dimensionless drain parameter μ is based on the assumption of a smear zone with constantly reduced permeability (Hansbo 1981; Walker and Indraratna 2007). Due to the lack of actual laboratory and on-site test data of q_{w0}, it is assumed that the initial discharge capacity q_{w0} at each depth is the same in these two cases.

4.1. Large scale model test

Large scale model tests to assess the consolidation and long-term performance of PVDs were reported by Deng et al. (2017); the soft soil to be tested came from the Ningbo Rail Transit project. The physical model is 0.5 m in diameter by 1 m high so it can be considered as a unit cell with a single layer. The loading process is shown in Fig. 3. The soil parameters used in the model came from Deng et al. (2017), i.e., $k_v = 2.17 \times 10^{-9}$ m/s, $k_h = 3 \times 10^{-9}$ m/s and $m_v = 8 \times 10^{-4}$ m^2/kN.

The parameters related to the vertical drain are used with respect to Deng et al. (2017): (a) the geometrical parameters are $d_e = 0.5$ m, $d_s = 0.1$ m, $d_w = 0.052$ m, $n = r_e/r_w = 9.615$, $s = r_s/r_w = 1.923$, and $l = H = 1$ m; (b) the permeability ratio is $k_h/k_s = 1.2$ and (c) the discharge capacity parameters are $q_{w0} = 3$ cm^3/s (or 0.2592 m^3/day), $\omega = 4.1 \times 10^{-6}$ s^{-1} (or 0.3542 day^{-1}), $t_c = 0$ days. The permeability ratio k_h/k_s in Deng et al. (2017) is 1, because they considered the soil was remoulded that does not have significant difference in its structure over different directions. However, despite using remoulded soil, the installation of a drain (i.e., smear effect) would certainly reduce its permeability of soil; this current study therefore assumes $k_h/k_s > 1$, i.e., 1.2. Note also that q_w is assumed to decay immediately with respect to Deng et al (2017).

Applying Eqs. (25) and (67), the theoretical settlement was obtained, where $Y = 0$ under the premise of $t_c = 0$ days. Fig. 3 shows the

Table 2
Layer properties for modelling of Saga Airport test embankment.

Depth (m)	$m_v/\overline{m}_v$	$k_v/\overline{k}_v$	η/η
0	0.56	4.32	4.32
1	0.53	4.32	4.32
1	0.86	2.16	2.16
4	0.86	2.16	2.16
4	0.05	164.77	109.85
5.6	0.05	164.77	109.85
5.6	1.00	1.00	1.00
21	0.62	1.00	1.00
21	0.03	164.77	109.85
23.7	0.03	164.77	109.85
23.7	0.43	1.00	1.00
25	0.48	1.00	1.00

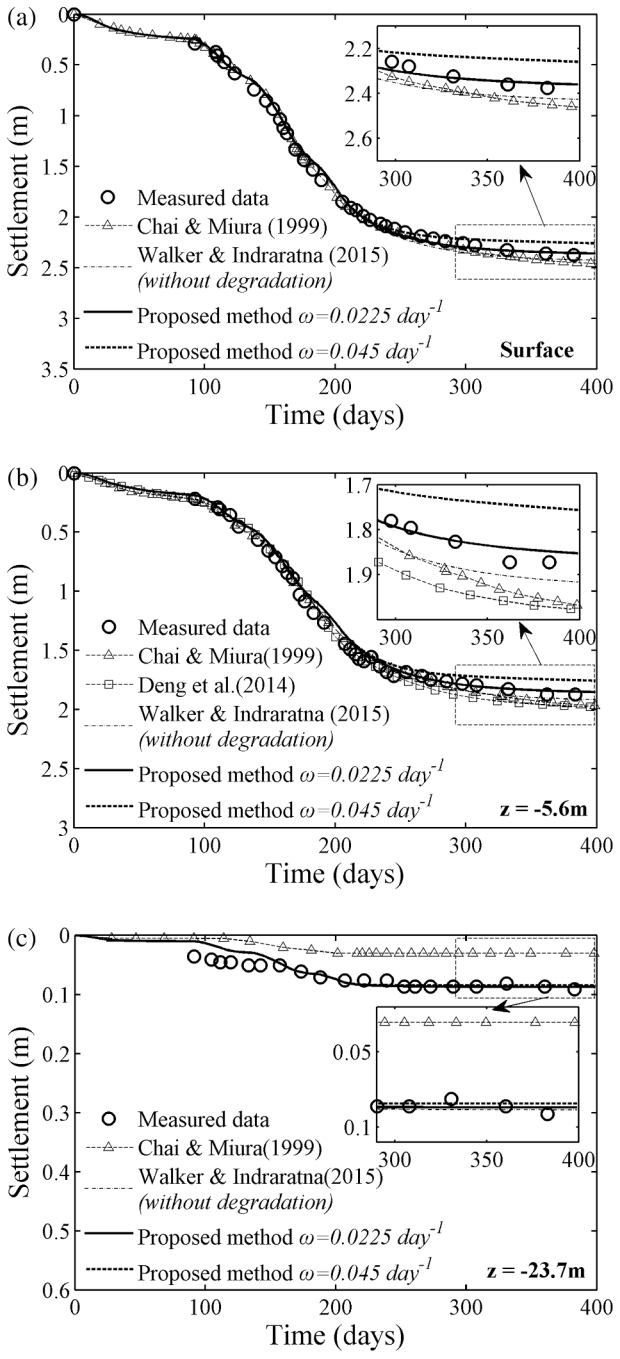

Fig. 5. . Settlement of Saga Airport test embankment: (a) surface; (b) at depth z = -5.6 m; (c) at depth z = –23.7 m.

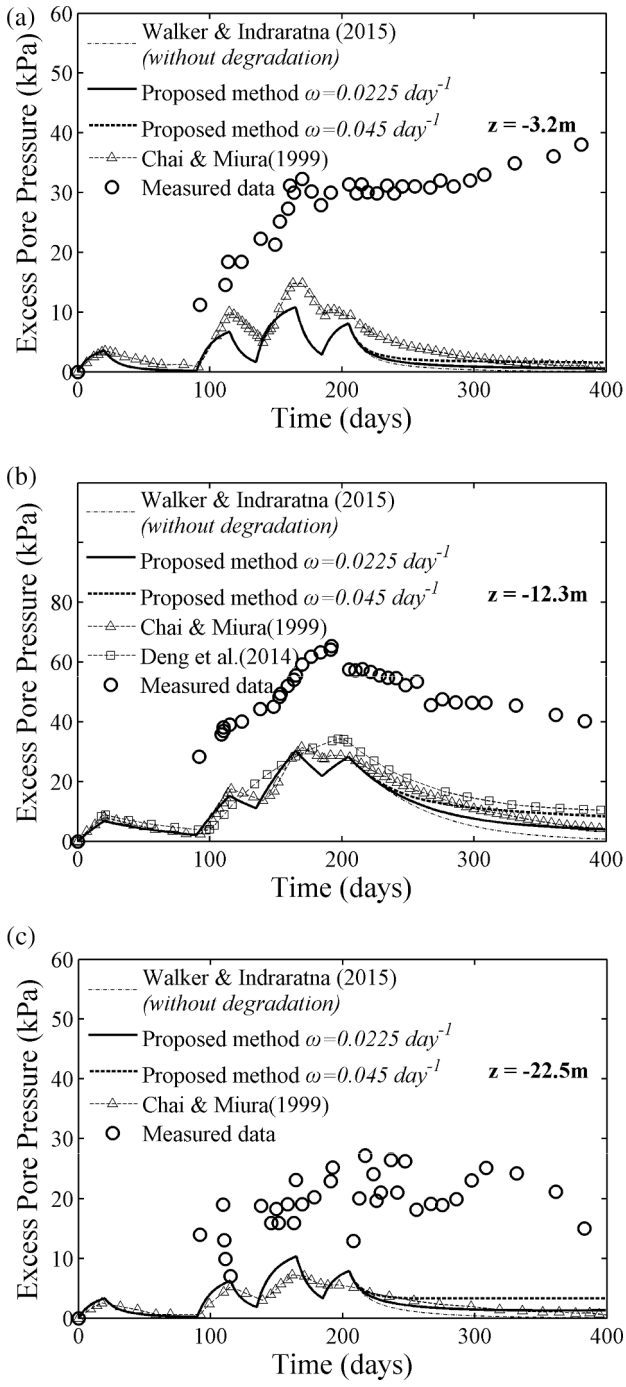

Fig. 6. . Comparison of EPWPs of Saga Airport test embankment (with original measurement): (a) at depth z = -3.2 m; (b) at depth z = -12.3 m; (c) at depth z = –22.5 m.

comparison between the measured and theoretical results where 40 series terms (i.e., $N = 40$ for numerically solving Eq. (67)) were used in the current spectral method. It is obvious that the calculated settlement that does not consider drain degradation begins to deviate from the experimental data after about 15 days. The difference between the experimental data and conventional prediction (i.e., without consideration of drain degradation) reaches about 13.0% at 25 days of consolidation. When drain degradation is considered, the settlement calculated by the proposed method is consistent with the measured result, and is more accurate than the analytical result obtained by Deng et al. (2017), especially in the later stages of consolidation. Specifically, the predicted

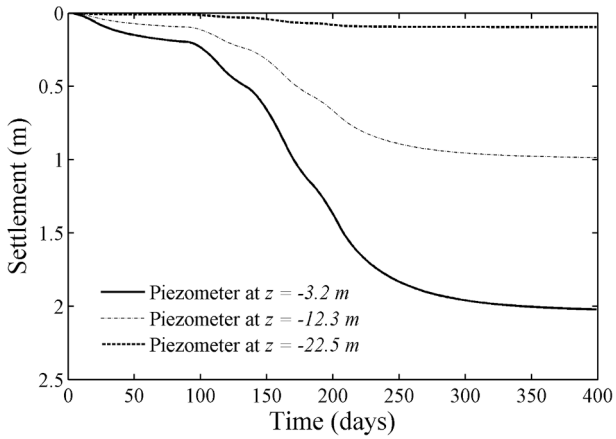

Fig. 7. . The settlement at the depth of 3 different piezometers calculated by the current study for Saga airport embankment.

settlement by the current solution agrees very well with the experimental data at about 35 days of consolidation, with an error of about 0.4%, whereas the result of Deng et al. (2017) has a deviation of nearly 2.7%. This result indicates a high accuracy of the proposed method, and the importance of considering drain degradation in calculating the radial consolidation of soil.

4.2. A soft subsoil test embankment at Saga Airport improved with PVD

The soft subsoil test embankment at Saga Airport improved with PVD was reported by Bergado et al. (1996); it was then predicted analytically by Chai and Miura (1999) and Deng et al. (2014) who considered drain degradation. Saga Airport is located 13 km south of the city of Saga and close to Ariake Bay. The reclaimed deposit mainly consists of soft and highly compressible Ariake clay. The base of the test embankment is 71 m by 71 m at the bottom and 25 m by 25 m at the top. The preloading construction process is shown in Fig. 4. The embankment was ramp loaded with filling rate of 0.03 m/day, and the final fill height for the surcharge preloading was 3.5 m. The unit weight of the fill material was 20 kN/m^3. The sub-soil can be divided into six sub-layers, and the parameters for each layer refer to those of Chai and Miura (1999), as given in Table 1. Note that the compressibility parameters are based on the Cam-clay compressibility properties given by (Chai and Miura 1999). The properties of the layers used to model the Saga Airport test embankment are given in Table 2.

The parameters related to the vertical drain are as follows: (a) the geometrical parameters are $d_e = 1.7$ m, $d_s = 0.3$ m, $d_w = 0.0483$ m, $n = r_e/r_w = 35.2$, $s = r_s/r_w = 6.2$, and $l = H = 25$ m, and (b) the permeability ratio is $k_h/k_s = 10.0$. The initial discharge capacity q_{w0} ranges from 200 to 2000 m^3/year (Deng et al. 2014). In this study, q_{w0} was assumed to be 300 m^3/year (or 0.8219 m^3/day) in all layers. The reduced discharge capacity of PVDs over time was measured by Chai and Miura (1999), and the degradation rate ω was determined as 2.6×10^{-7} s^{-1} (or 0.0225 day^{-1}) by Deng et al. (2014), so it was also adopted in this study. In addition, two other degradation rates were also considered, one of which did not include degradation ($\omega = 0$ day^{-1}), i.e., the solution of Walker and Indraratna (2015) based on the spectral method, and the other incorporating a larger degradation rate ($\omega = 0.045$ day^{-1}). The field data (Chai and Miura 1999) show that settlement developed quickly for the first 205 days and then decreased rapidly, which implies that the large deformation (i.e., 1.85 m ≈ 7.4% vertical strain) is likely to cause the PVDs to bend, kink and fold, which could reduce the drainage efficiency and retarded consolidation. It can therefore be assumed that the start time of degradation t_c was approximately 205 days, so $A(t)$ in this case was calculated by Eq. (25).

The settlement and EPWP calculations are mainly based on the

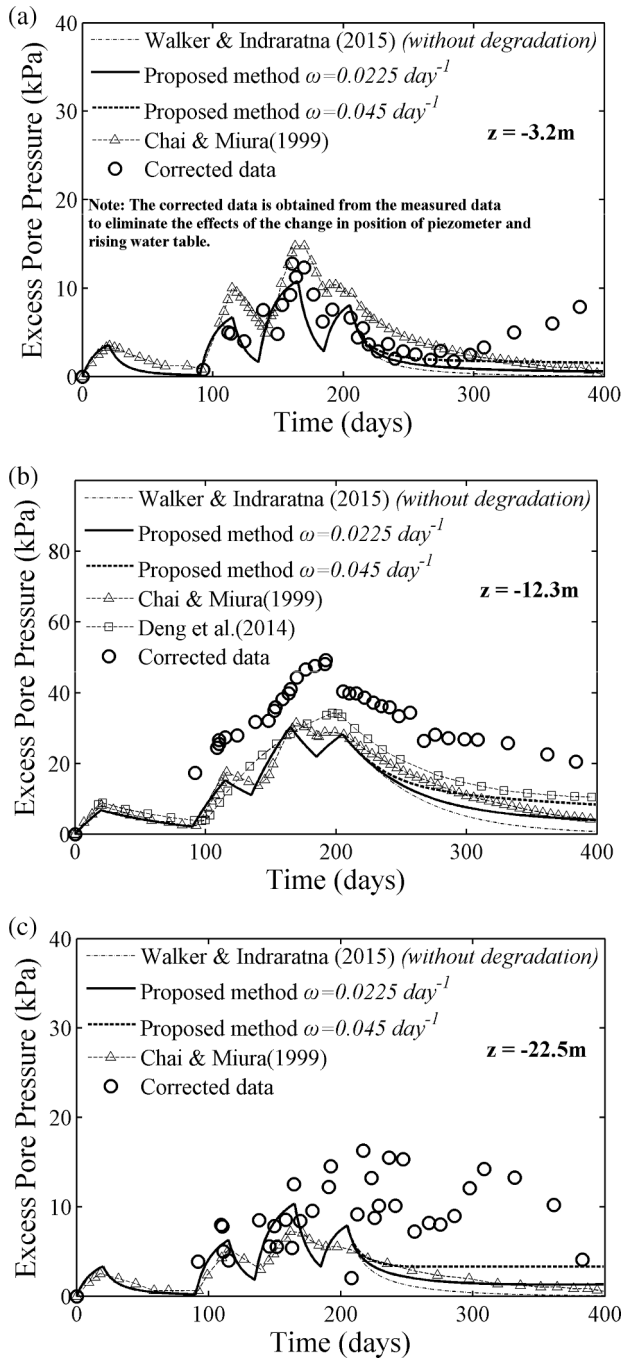

Fig. 8. . Comparison of EPWPs of Saga Airport test embankment (with corrected data): (a) at depth z = -3.2 m; (b) at depth z = -12.3 m; (c) at depth z = –22.5 m.

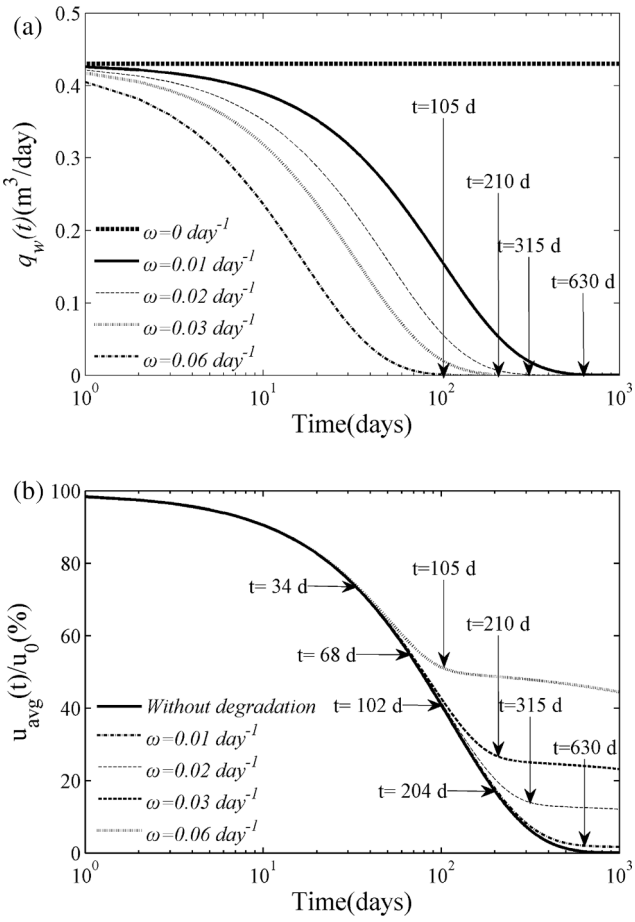

Fig. 9. . (a) Reduction of discharge capacity with different ω; (b) Comparison of the consolidation with different ω.

parameters given by Chai and Miura (1999), which were calculated by Eqs. (10), (25) and (67) (20 series terms were used), as shown in Figs. 5 and 6. The settlements measured and calculated at three different depths are shown in Fig. 5 as a comparison with previous predictions. Fig. 5(a) and (b) show that when drain degradation is ignored ($\omega = 0$ day^{-1}), the settlements predicted by the current study at the surface and at a depth of z = -5.6 m are similar to those of Chai and Miura (1999) and Deng et al. (2014), and are larger than the actual measurements, especially in the later stage of consolidation. When drain degradation is considered using $\omega = 0.0225$ day^{-1}, a better agreement with the measured data can be obtained. Whereas previous models have the smallest difference of about 3.0% and 3.6% at 360 days from the field data for the surface and depth of z = -5.6 m, respectively; the current predictions reduce these deviations to about 0.5% and 1.3%, respectively. The study also indicates that when the degradation rate is overestimated, i.e., $\omega = 0.045$ day^{-1}, the predicted settlements are smaller than the actual values.

For settlement at a deeper depth of z = –23.7 m (Fig. 5**(c)**), the predictions by Chai and Miura (1999) have underestimated the measured data, but the result calculated by the spectral method provides a more accurate prediction. For example, the difference between the predicted and measured data at 360 days decreased to about 0.7% using the current method. This is because, the current method is based on a rigorous mathematical framework where soil properties at different layers can now be incorporated explicitly in the governing equation of soil consolidation, which is distinctly different from the past solution methods. However, the settlement predicted using the three different rates of degradation do not differ at this depth, because effective stress and associated settlement at this deep level are at a small scale.

Fig. 6 compares the predicted EPWP by the proposed solution and measured data to other simulations. Note here that the predicted results are less than the measured data, as are the results in Chai and Miura (1999) and Deng et al. (2014). Deng et al. (2014) explained that it may be caused by fluctuations at groundwater level, disturbance by construction vehicles, and the locations and methods used to place the instruments in position. To better represent the results in this current study, the measured values have therefore been corrected by eliminating the effects of the piezometer positions and the static hydraulic pressure induced by the water table. Settlement of the piezometers at three different depths was calculated using the proposed method and the results can been shown in Fig. 7. Due to the lack of on-site groundwater level monitoring records, the average change of groundwater level was

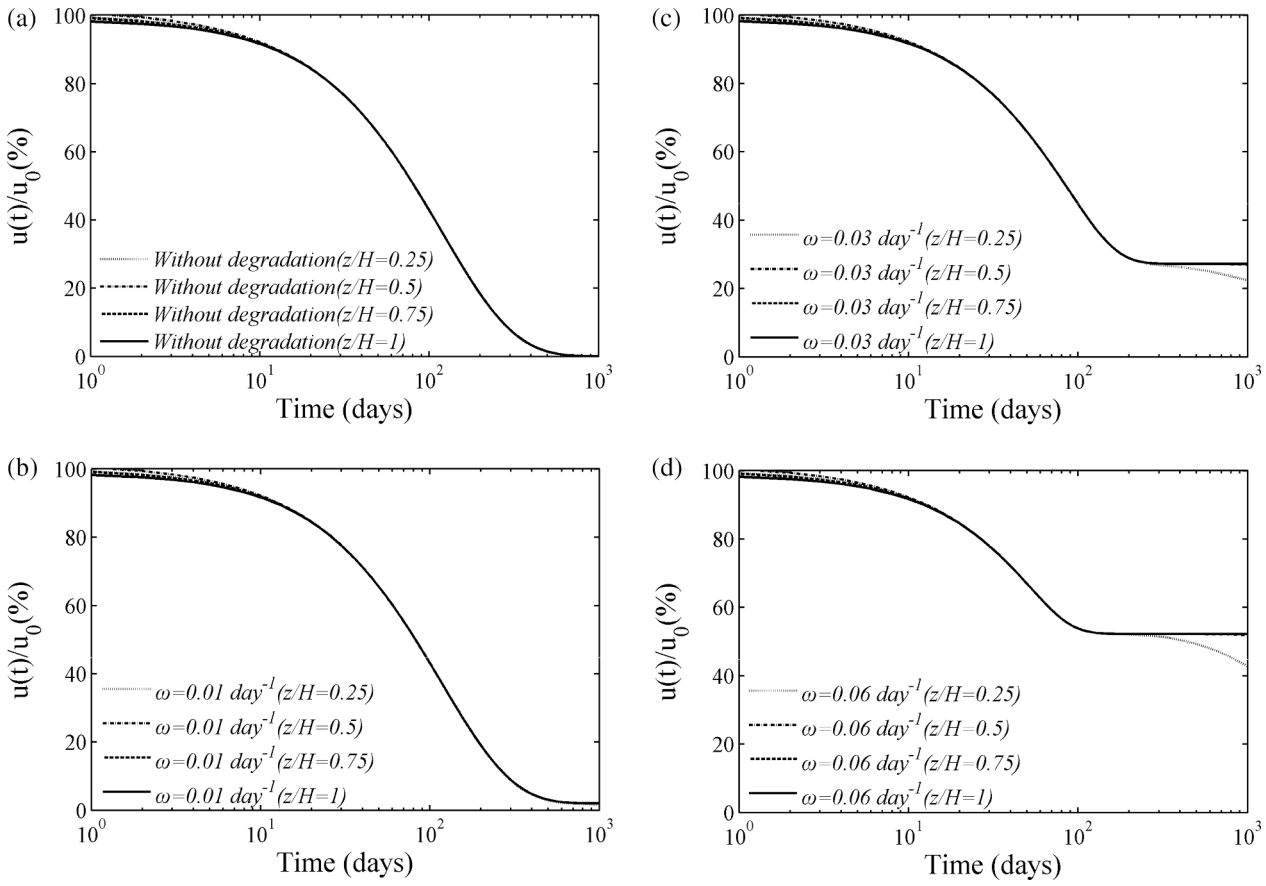

Fig. 10. . Dissipations of EPWPs at different depths with different ω: (a) $\omega = 0$ day^{-1}; (b) $\omega = 0.01$ day^{-1}; (c) $\omega = 0.03$ day^{-1}; (d) $\omega = 0.06$ day^{-1}.

assumed to be 1 m, and this produced approximately 10 kPa of static hydraulic pressure.

Fig. 8 shows the results predicted by the current and previous solutions when compared to the corrected field data. The results show that the calculated pore water pressures are relatively close to the corrected data (i.e., eliminate the effects of the piezometer positions and the static hydraulic pressure induced by the water table), and have similar trends with other predictions; in fact, the values of EPWP predicted in the layer of clay Ac1 by the proposed method are closer to the measured data. Moreover, when drain degradation is considered by using $\omega = 0.0225$ day^{-1}, the overall result predicted has a similar dissipation trend as the measured pore water pressure, especially in the main layer of clay Ac2 (at depth of $z = -12.3$ m), but when drain degradation is not considered ($\omega = 0$ day^{-1}), the pore water pressures dissipate much faster. However, when the rate of degradation is too big ($\omega = 0.045$ day^{-1}), the pore water pressures dissipate much more slowly. The result not only indicates how accurately this approach can capture the influence that degraded drains have on the consolidation of multi-layered soil, it also highlights the need to properly evaluate drain degradation in practice.

The results in the above two verification cases indicate that the degradation of q_w has a significant effect on the consolidation of ground installed with PVD, especially in the later stages where the degradation of PVDs usually becomes more critical. It is therefore recommended that the degradation of q_w during consolidation should be considered when designing PVD-ground improvements, particularly where conditions such as large strain consolidation could seriously degrade the drains. This proposed solution based on the spectral method is suitable for analysing vertical and radial consolidation in more realistic conditions such as multi-layered soils and multi-stage loading associated with drain degradation.

5. Influence of degradation parameters on consolidation

Parameters such as the degradation rate ω and the beginning time of degradation t_c have a huge impact on predicting the consolidation of soil improved with PVD. Since the feasibility of the proposed model has been verified in the previous section, the impact that the degradation parameters have on consolidation is further investigated in this section by considering the vertical and radial consolidation of a unit cell by a PVD incorporating the decay of q_w.

In order to focus on the study of the effect of drain degradation, the soil properties in this analysis are assumed to be as follows. (1) The soil properties are $k_v = k_h = 1 \times 10^{-9}$ m/s, $k_h/k_s = 3$ and $m_v = 8 \times 10^{-2}$ m^2/kN; (2) The geometrical parameters are $d_e = 0.6$ m, $d_s = 0.22$ m, $d_w = 0.064$ m, $n = r_e/r_w = 9.375$, $s = r_s/r_w = 3.4375$, and $l = H = 10$ m; (3) The initial discharge capacity $q_{w0} = 0.43$ m^3/day is where q_w is assumed to only vary with time t. An instantaneous load of 100 kPa is placed on top of the unit cell while ω and t_c are changed in different combinations in this paper.

5.1. Degradation rate ω

To study the impact of degradation rate ω, the start time of degradation t_c was set at 0 days. Five different rates of degradation ω were studied: (i) $\omega = 0$ day^{-1}; (ii) $\omega = 0.01$ day^{-1}; (iii) $\omega = 0.02$ day^{-1}; (iv) $\omega = 0.03$ day^{-1}; (v) $\omega = 0.06$ day^{-1}. Fig. 9 shows the consolidation of a degradable drain subjects to different degradation rates; it shows that the dissipation curves of average EPWP when considering different degradation rates deviate from the dissipation curves without causing any degradation. The deviation times are approximately 34 days, 68 days, 102 days and 204 days for $\omega = 0.06$ day^{-1}, $\omega = 0.03$ day^{-1}, $\omega = 0.02$ day^{-1} and $\omega = 0.01$ day^{-1}, respectively. This means the dissipation

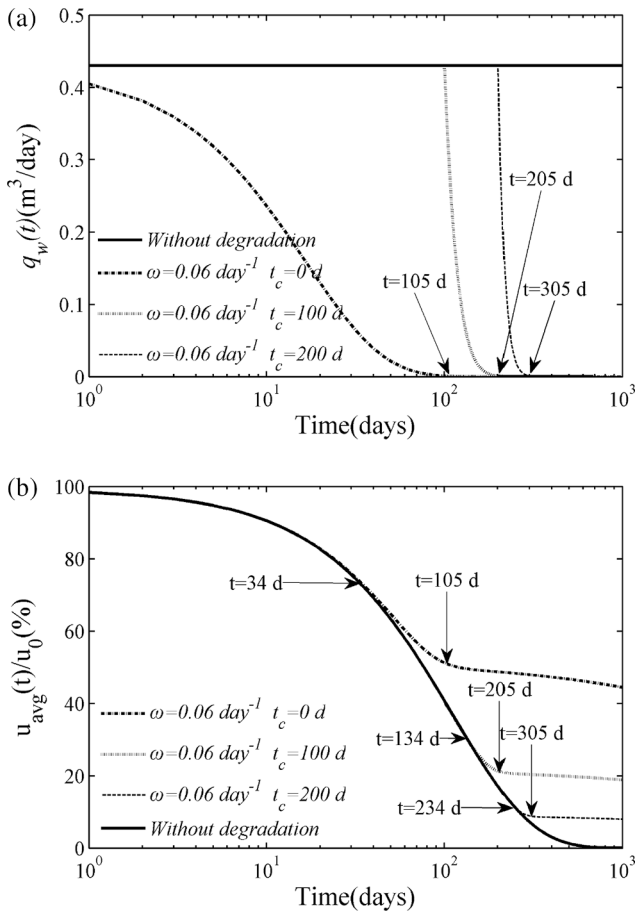

Fig. 11. . (a) Reduction of discharge capacity with different t_c with the same ω; (b) Comparison of the consolidation with different t_c.

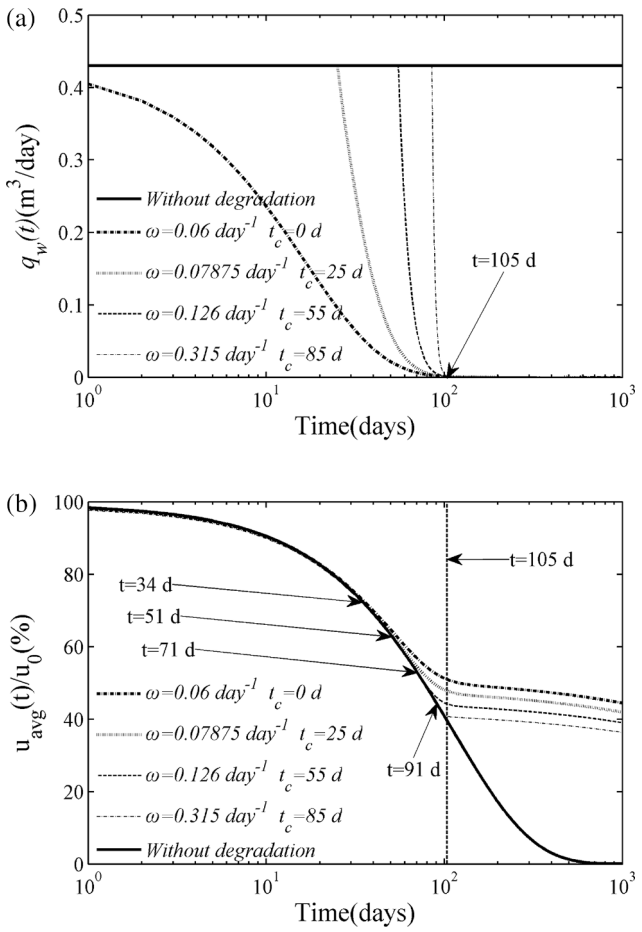

Fig. 12. . (a) Reduction of discharge capacity with different ω and t_c; (b) Comparison of the consolidation with different combinations of ω and t_c.

of EPWPs is impeded significantly when the q_w decays to a certain extent; for instance, the impedance threshold for q_w in this study is approximately 0.056 m^3/day. Moreover, Fig. 9 also shows that the dissipation curves of the average EPWP are retarded when the q_w decreases to a critical value. The consolidation curves turn into a critical state of decay after approximately 105 days, 210 days, 315 days and 630 days for $\omega = 0.06$ day^{-1}, $\omega = 0.03$ day^{-1}, $\omega = 0.02$ day^{-1} and $\omega = 0.01$ day^{-1}, respectively. In this study, the critical value of the q_w is approximately 7.9×10^{-4} m^3/day. This critical state of decay indicates that as the q_w of the drain becomes very small, the dissipation of pore water pressure along the radial direction is seriously affected, thus retarding the radial consolidation. Moreover, Fig. 9 also shows that as the degradation rate increases, the consolidation rate decreases.

Fig. 10 shows consolidation at different depths with different rates of degradation. Note that the normalised depth z/H was used, where z is the depth from the surface, and H is the total depth of soil. Apparently, as the rates of degradation increases it has more impact on the dissipation of EPWPs at different depths, however, in the less severe cases of degradation where $\omega = 0$ and 0.01 day^{-1}, the difference in consolidation at each depth is small and the dissipation curves at various depths are almost coincident. In a more serious case (i.e., a larger degradation rate) where $\omega = 0.03$ and 0.06 day^{-1}, the dissipation curves below 5 m are almost the same, but they are much slower than that at 2.5 m. This tendency is more pronounced at higher rates of degradation, which implies that an increasing rate of degradation has a lot of influence on the overall average dissipation of EPWP, and this effect is more significant in a deeper soil layers.

To obtain the rate of degradation more reliably in practice, so that the influence of other factors can be delineated, the direct measurement of discharge flow rate through a soil-drain system with time is required. This experimental approach has been applied successfully in the past (e.g. Chai and Miura 1999, Kim et al. 2011; Bo et al. 2016; Nguyen et al. 2018).

5.2. the start time of drain degradation

Two cases were set up to study the impact of the start time of degradation t_c:

(1) The rate of degradation $\omega = 0.06$ day^{-1} remains constant and three separate start times where $t_c = 0$, 100 and 200 days are considered;

(2) To reach the critical q_w (approximately 7.9×10^{-4} m^3/day) at the same time where $t = 105$ days, three combined degradation rates and start times of degradation are investigated, i.e., (a) $\omega = 0.06$ day^{-1} and $t_c = 0$ days; (b) $\omega = 0.07875$ day^{-1} and $t_c = 25$ days; (c) $\omega = 0.126$ day^{-1} and $t_c = 55$ days; (d) $\omega = 0.315$ day^{-1} and $t_c = 85$ days.

Fig. 11 shows the comparison between the dissipation of EPWP of a degradable drain subjected to the same rate of degradation but with different start times of degradation. It is observed that all the dissipation curves with different start times of degradation and the same degradation rate ($\omega = 0.06$ day^{-1}) deviate from that without degradation after 34 days of degradation. Fig. 11 also shows that regardless of when degradation commences, if the degradation rate remains the same, the dissipation curves become retarded after the same decay time. In this case, all the dissipation curves were retarded after 105 days of degradation because q_w is below 7.9×10^{-4} m^3/day.

Different decay rates and start times of degradation were also examined in order to understand how varying the parameters of degradation could affect consolidation. In this case, q_w was designed to

reduce to a critical value at the same time ($t = 105$ days), as shown in Fig. 12. The results show that dissipation curves with different rates of decay and start times of degradation deviate from the dissipation curves without degradation at different times, i.e., 34 days, 51 days, 71 days and 71 days for (i) ($\omega = 0.06$ day^{-1} and $t_c = 0$ days), (ii) ($\omega = 0.07875$ day^{-1} and $t_c = 25$ days), (iii) ($\omega = 0.126$ day^{-1} and $t_c = 55$ days) and (iv) ($\omega = 0.315$ day^{-1} and $t_c = 85$ days), respectively. This means that regardless of when degradation begins or what the rate of decay is, as long as q_w decays to the impeded threshold the dissipation of EPWP is largely impeded. These results also show that dissipation curves with different rates of decay and start times of degradation are retarded after approximately 105 days because q_w is below the critical value. Moreover, Figs. 11 and 12 show that the earlier the drains begin to degrade (i.e, $t_c = 0$ days), the lower will be the rate of consolidation.

The above analysis reveals that an increasing rate of degradation and a shorter time before degradation begins will reduce the rate of consolidation. Furthermore, when q_w has degraded to an impeded threshold the dissipation of EPWP will be obstructed, and when the critical value is reached, the rate of consolidation will be retarded. The threshold of impedance and the critical value of q_w are related to factors such as the horizontal permeability coefficients (k_h and k_s), and the geometric parameters of the unit cell (d_w, d_e, d_s, l and H). In this study, the threshold of impedance and the critical values are approximately 0.056 m^3/day and 7.9 $\times$ 10^{-4} m^3/day, respectively.

6. Conclusion

In this paper, the authors have proposed a novel approach to describe the consolidation of multi-layered soil with respect to the degradation in discharge capacity of drains. Drains where the q_w varies with time and depth have been incorporated into the theory of soil consolidation considering both vertical and radial drainages over different soil layers. The mathematical technique using the spectral method was adopted to solve the governing equations to determine the multilayer soil consolidation. The following conclusions could be drawn:

(1) The major advantage of the proposed spectral solution is its rigorous mathematical formation that enables realistic variables such as the degraded drains and inhomogeneous soil properties to be incorporated into the governing equations of soil consolidation. The application of this method to previous laboratory and field studies showed considerable improvement in the accuracy of prediction. For example, at Saga Airport (Chai and Miura, 1999), the proposed solution reduced the difference between the field measurements and predictions of surface settlement from about 3.0% to just 0.5% after 1 year. In addition, the proposed method can capture well the detailed difference in consolidation that different soil layers can have due to varying drain and soil properties with time and depth.

(2) The degradation of drains can adversely affect the consolidation of soil, especially in later stages when the reduced discharge capacity becomes critical. Applying the proposed method to a field embankment (i.e., Saga Airport 1999) showed that the prediction based on the spectral method could match the measured data better when a degradation rate of 0.0225 day^{-1} was considered.

(3) Increasing degradation rate combined with an earlier start time for degradation t_c can result in a greater impact on the overall average dissipation of EPWP, and thus reduce the rate of consolidation, especially in deeper soil layers.

(4) The reduced discharge capacity has an impedance threshold and critical value to which the more reduction can seriously obstruct the dissipation of EPWP and retard the rate of consolidation, respectively. The impedance threshold and critical value of q_w are independent of the rate and start time of degradation.

CRediT authorship contribution statement

Bin-Hua Xu: Conceptualization, Methodology, Software, Data curation, Writing - original draft, Visualization. **Buddhima Indraratna:** Validation, Resources, Supervision, Project administration, Writing - review & editing. **Thanh Trung Nguyen:** Conceptualization, Methodology, Validation, Investigation, Formal analysis, Visualization, Writing - review & editing. **Rohan Walker:** Validation, Formal analysis, Writing - review & editing.

Declaration of Competing Interest

The authors declare that they have no known competing financial interests or personal relationships that could have appeared to influence the work reported in this paper.

Acknowledgements

This research is sponsored by the National Key Research and Development Program of China (2018YFC1508500), the China Scholarship Council (CSC) (Grant No. 201906710072). The Authors also acknowledge the support from the Transport Research Centre, University of Technology Sydney.

Appendix A:. Solution of governing equation by spectral method and corresponding matrix expressions

A.1: Solution of governing equation by spectral method

The test functions for the spectral Galerkin method are the same as the basis ones. By using the weighted residual method, the non-homogeneous governing differential equation Eqs. (1) and (2) in matrix form are:

$$\boldsymbol{\Gamma}\frac{\partial \boldsymbol{A}}{\partial t} + \boldsymbol{\psi A} + \boldsymbol{\xi A} = \boldsymbol{\theta} + \boldsymbol{\psi B} \tag{26}$$

$$\boldsymbol{\psi B} + \boldsymbol{\chi B} = \boldsymbol{\psi A} \tag{27}$$

$$\Gamma_{ij} = \int_0^1 \frac{m_v}{\overline{\overline{m}}_v}\phi_i\phi_j dZ \tag{28}$$

$$\psi_{ij} = dT_h \int_0^1 \frac{\eta}{\overline{\overline{\eta}}}\phi_i\phi_j dZ \tag{29}$$

$$\zeta_{ij} = -dT_v \int_0^1 \frac{\partial}{\partial Z}\left(\frac{k_v}{\overline{\overline{k}}_v}\frac{\partial \phi_j}{\partial Z}\right)\phi_i dZ \tag{30}$$

$$\chi_{ij} = -dT_w \int_0^1 \frac{\partial}{\partial Z}\left(q_w \frac{\partial \phi_j}{\partial Z}\right)\phi_i dZ \tag{31}$$

$$\theta_i = \int_0^1 \phi_i \frac{m_v}{\overline{m}_v}\frac{\partial \overline{\sigma}}{\partial t} dZ \tag{32}$$

Insolating $\boldsymbol{B}$ from Eq. (27) and substituting it into Eq. (26) gives:

$$\boldsymbol{\Gamma}\frac{\partial \boldsymbol{A}}{\partial t} + \left(\boldsymbol{\psi} + \boldsymbol{\zeta} - \boldsymbol{\psi}(\boldsymbol{\psi}+\boldsymbol{\chi})^{-1}\boldsymbol{\psi}\right)\boldsymbol{A} = \boldsymbol{\theta} \tag{33}$$

By using the method of variation of parameters, the solution to the non-homogeneous Eq. (26) can be found using the initial condition $\boldsymbol{A}(0) = 0$:

$$\boldsymbol{A}(t) = \boldsymbol{A}(0)e^{-\int_0^t \boldsymbol{\Gamma}^{-1}\left(\boldsymbol{\psi}+\boldsymbol{\zeta}-\boldsymbol{\psi}(\boldsymbol{\psi}+\boldsymbol{\chi})^{-1}\boldsymbol{\psi}\right)d\tau} + e^{-\int_0^t \boldsymbol{\Gamma}^{-1}\left(\boldsymbol{\psi}+\boldsymbol{\zeta}-\boldsymbol{\psi}(\boldsymbol{\psi}+\boldsymbol{\chi})^{-1}\boldsymbol{\psi}\right)d\tau}\int_0^t e^{\int_0^\tau \boldsymbol{\Gamma}^{-1}\left(\boldsymbol{\psi}+\boldsymbol{\zeta}-\boldsymbol{\psi}(\boldsymbol{\psi}+\boldsymbol{\chi})^{-1}\boldsymbol{\psi}\right)dt}\boldsymbol{\Gamma}^{-1}\boldsymbol{\theta}d\tau \tag{34}$$

$$\boldsymbol{A}(t) = e^{-\int_0^t \boldsymbol{\Gamma}^{-1}\left(\boldsymbol{\psi}+\boldsymbol{\zeta}-\boldsymbol{\psi}(\boldsymbol{\psi}+\boldsymbol{\chi})^{-1}\boldsymbol{\psi}\right)d\tau}\int_0^t e^{\int_0^\tau \boldsymbol{\Gamma}^{-1}\left(\boldsymbol{\psi}+\boldsymbol{\zeta}-\boldsymbol{\psi}(\boldsymbol{\psi}+\boldsymbol{\chi})^{-1}\boldsymbol{\psi}\right)dt}\boldsymbol{\Gamma}^{-1}\boldsymbol{\theta}d\tau \tag{35}$$

Then Eq. (10) is obtained.

A.2: Explicit expressions of matrix elements

This section represents the integrals and explicit matrix element expressions in the analytical solution. When calculating the integrations in Eqs. (28)-(32), some products of the trigonometric and linear polynomial functions with a similar form were integrated. To present the equations for $\boldsymbol{\Gamma}$, $\boldsymbol{\psi}$, $\boldsymbol{\zeta}$, $\boldsymbol{\chi}$ and $\boldsymbol{\theta}$ in a concise manner, some shorthand notations are adopted as shown below:

$$SN(\alpha, \beta^k) = \frac{\alpha^{l+1}sin[\beta Z_{l+1}] - \alpha^l sin[\beta Z_l]}{\beta^k} \tag{36}$$

$$CS(\alpha, \beta^k) = \frac{\alpha^{l+1}cos[\beta Z_{l+1}] - \alpha^l cos[\beta Z_l]}{\beta^k} \tag{37}$$

$$M^- = M_i - M_j \tag{38}$$

$$M^+ = M_i + M_j \tag{39}$$

$$\Delta a = a^{l+1} - a^l \tag{40}$$

Note that Δ is an operator in the Z direction, where the superscript l represents parameters (i.e., soil parameters, discharge capacity parameters) at the top of the l^{th} layer.

The $\boldsymbol{\Gamma}$ matrix is related to the compressibility of the soil. As shown in Eq. (28), the contribution made by the l^{th} layer of soil to Γ_{ij} is given by:

$$\Gamma_{ij}(l) = \int_{Z_l}^{Z_{l+1}} m_v^l(Z)\phi_i\phi_j dZ \tag{41}$$

The diagonal ($i = j$) and the off diagonal ($i \neq j$) elements of $\boldsymbol{\Gamma}$ have different expressions, which have the same expressions as Walker and Indraratna (2009). For $i = j$, the diagonal elements of $\Gamma_{ij}(l)$ are calculated with:

$$\Gamma_{ij}(l) = \frac{1}{2}\left(\frac{\Delta Z}{2}\left(m_v^{l+1} + m_v^l\right) - \frac{\Delta m_v}{\Delta Z}CS\left[1, (M^+)^2\right] - SN\left[m_v, (M^+)^1\right]\right) \tag{42}$$

For $i \neq j$, the off diagonal elements of $\Gamma_{ij}(l)$ are calculated with:

$$\Gamma_{ij}(l) = \frac{1}{2}\left(\frac{\Delta m_v}{\Delta Z}\left(CS\left[1, (M^-)^2\right] - CS\left[1, (M^+)^2\right]\right) + SN\left[m_v, (M^-)^1\right] - SN\left[m_v, (M^+)^1\right]\right) \tag{43}$$

In the interface layers where $Z_l \rightarrow Z_{l+1}$, the limits of Eqs. (42)-(43) are both zero.

The $\boldsymbol{\psi}$ matrix is related to the radial drainage properties of the soil. As shown in Eq. (29), the contribution made by the l^{th} layer of soil to ψ_{ij} is given by:

$$\psi_{ij}(l) = \int_{Z_l}^{Z_{l+1}} dT_h \eta^l(Z)\phi_i\phi_j dZ \tag{44}$$

For $i = j$, the diagonal elements of $\psi_{ij}(l)$ are calculated with:

$$\psi_{ij}(l) = \frac{dT_h}{2}\left(\frac{\Delta Z}{2}\left(\eta^{l+1} + \eta^l\right) - \frac{\Delta \eta}{\Delta Z}CS\left[1, (M^+)^2\right] - SN\left[\eta, (M^+)^1\right]\right) \tag{45}$$

For $i \neq j$, the off diagonal elements of $\psi_{ij}(l)$ are calculated with:

$$\psi_{ij}(l) = \frac{dT_h}{2}\left(\frac{\Delta \eta}{\Delta Z}\left(CS\left[1, (M^-)^2\right] - CS\left[1, (M^+)^2\right]\right) + SN\left[\eta, (M^-)^1\right] - SN\left[\eta, (M^+)^1\right]\right) \tag{46}$$

In the interface layers where $Z_l \rightarrow Z_{l+1}$, the limit of Eqs. (45)-(46) is zero.

The $\boldsymbol{\zeta}$ matrix is related to the vertical drainage properties of the soil. As presented in Eq. (30), the contribution made by the l^{th} layer of soil to ζ_{ij} is

given by:

$$\zeta_{ij}(l) = -\int_{Z_l}^{Z_{l+1}} dT_v \frac{\partial}{\partial Z}\left(k_v^l(Z)\frac{\partial \phi_j}{\partial Z}\right)\phi_i dZ \tag{47}$$

For $i = j$, the diagonal elements of $\zeta_{ij}(l)$ are calculated with:

$$\zeta_{ij}(l) = \frac{1}{2}dT_v M_j^2\left(\frac{\Delta Z}{2}\left(k_v^l + k_v^{l+1}\right) - SN\left[k_v, (M^+)^1\right] + \frac{\Delta k_v}{\Delta Z}CS\left[1, (M^+)^2\right]\right) \tag{48}$$

For $i \neq j$, the off diagonal elements of $\zeta_{ij}(l)$ are calculated with:

$$\zeta_{ij}(l) = \frac{1}{2}dT_v\left(\frac{\Delta k_v M_j M_i}{\Delta Z}\left(CS\left[1, (M^-)^2\right] + CS\left[1, (M^+)^2\right]\right) + M_j^2\left(SN\left[k_v, (M^-)^1\right] - SN\left[k_v, (M^+)^1\right]\right)\right) \tag{49}$$

In the interface layers where $Z_l \rightarrow Z_{l+1}$, the limit of the elements in Eqs. (48)-(49) are the same and are described as:

$$\zeta_{ij}(l) = -dT_v M_j \Delta k_v cos\left(M_j Z_l\right) sin\left(M_i Z_l\right) \tag{50}$$

The χ matrix is related to the properties of the drain. As presented in Eq. (31), the contribution made by the l^{th} layer of soil to χ_{ij} is given by:

$$\chi_{ij}(l) = -dT_w \int_{Z_l}^{Z_{l+1}} \frac{\partial}{\partial Z}\left(q_w^l(Z,t)\frac{\partial \phi_j}{\partial Z}\right)\phi_i dZ \tag{51}$$

Then, $\chi_{ij}(l)$ can be described as:

$$\chi_{ij}(l) = -Q_w(t)dT_w \int_{Z_l}^{Z_{l+1}} \frac{\partial}{\partial Z}\left(Q_w^l(Z)\frac{\partial \phi_j}{\partial Z}\right)\phi_i dZ \tag{52}$$

Define $X_{ij}(l) = -dT_w \int_{Z_l}^{Z_{l+1}} \frac{\partial}{\partial Z}\left(Q_w^l(Z)\frac{\partial \phi_j}{\partial Z}\right)\phi_i dZ$, then $\chi_{ij}(l) = Q_w(t)X_{ij}(l)$. For $i = j$, the diagonal elements of $X_{ij}(l)$ are calculated with:

$$X_{ij}(l) = \frac{1}{2}dT_w M_j^2\left(\frac{\Delta Z}{2}\left(q_{w0}^l + q_{w0}^{l+1}\right) - SN\left[q_{w0}, (M^+)^1\right] + \frac{\Delta q_{w0}}{\Delta Z}CS\left[1, (M^+)^2\right]\right) \tag{53}$$

For $i \neq j$, the off diagonal elements of $X_{ij}(l)$ are calculated with:

$$X_{ij}(l) = \frac{1}{2}dT_w\left(\frac{\Delta q_{w0} M_j M_i}{\Delta Z}\left(CS\left[1, (M^-)^2\right] + CS\left[1, (M^+)^2\right]\right) + M_j^2\left(SN\left[q_{w0}, (M^-)^1\right] - SN\left[q_{w0}, (M^+)^1\right]\right)\right) \tag{54}$$

In the interface layers where $Z_l \rightarrow Z_{l+1}$, the limit of the elements in Eqs. (53)-(54) are the same and are described as:

$$X_{ij}(l) = -dT_w M_j \Delta q_{w0} cos\left(M_j Z_l\right) sin\left(M_i Z_l\right) \tag{55}$$

The θ matrix is related to the compressibility of the soil and the total stress. As presented in Eq. (32), the contribution made by the l^{th} layer of soil to θ_i in the s^{th} loading is given by:

$$\theta_i(l,s) = \int_{Z_l}^{Z_{l+1}} \phi_i m_v^l \frac{\partial \overline{\sigma}^{l,s}(Z,t)}{\partial t} dZ \tag{56}$$

Based on Eq. (14), $\partial \overline{\sigma}^l(Z,t)/\partial t$ can be described as:

$$\frac{\partial \overline{\sigma}^{l,s}(Z,t)}{\partial t} = \frac{\partial F_s(t)}{\partial t}\left(\overline{\sigma}^{l,s+1}(Z) - \overline{\sigma}^{l,s}(Z)\right) \tag{57}$$

where $F_s^{'}(t) = \partial F_s(t)/\partial t$ is given by:

$$F_s^{'}(t) = \begin{cases} \dfrac{1}{t_{s,1} - t_{s,0}} & \text{for } t_{s,0} < t_{s,1} \quad (ramp\ loading) \\ \delta\left(t - t_{s,1}\right) & \text{for } t_{s,0} = t_{s,1} \quad (instantaneous\ loading) \end{cases} \tag{58}$$

where $\delta(x)$ is the Dirac delta function. The contribution made by the l^{th} layer of soil to $\boldsymbol{\theta_i}$ in the s^{th} loading can be calculated by:

$$\theta_i(l,s) = F_s^{'}(t)\Theta_i(\overline{\sigma}^{l,s+1} - \overline{\sigma}^{l,s}, \Delta\overline{\sigma}^{s+1} - \Delta\overline{\sigma}^{s}, m_v) \tag{59}$$

where Θ can be defined by:

$$\Theta_i(\alpha,\beta,\delta) = \frac{1}{M_i}\left(\alpha\left(\frac{\Delta\delta}{\Delta Z}SN\left[1, (M_i)^1\right] - CS\left[m_v, (M_i)^0\right]\right) + \beta\left[\left(2\frac{\Delta\delta}{\Delta Z^2}CS\left[1, (M_i)^2\right]\right) + \frac{1}{\Delta Z}\left(SN\left[\delta, (M_i)^1\right] + \frac{\Delta\delta}{M_i}sin\left(M_i Z_{l+1}\right)\right) - \delta_{l+1}cos\left(M_i Z_{l+1}\right)\right]\right) \tag{60}$$

Define $\Theta_i(l,s) = \Theta_i(\overline{\sigma}^{l,s+1} - \overline{\sigma}^{l,s}, \Delta\overline{\sigma}^{s+1} - \Delta\overline{\sigma}^{s}, m_v)$, so $\theta_i(l,s) = F_s^{'}(t)\Theta_i(l,s)$.

In the interface layers where $Z_l \rightarrow Z_{l+1}$, the limit of Eq. (60) is zero.

If the number of layers is m, the final values for $\boldsymbol{\Gamma}$, $\boldsymbol{\psi}$, $\boldsymbol{\zeta}$, $\boldsymbol{X}$, $\boldsymbol{\chi}$, $\boldsymbol{\Theta}$ and $\boldsymbol{\theta}$ are given by adding the contribution of each layer of soil:

$$\Gamma_{ij} = \sum_{l=1}^{m} \Gamma_{ij}(l), \quad \psi_{ij} = \sum_{l=1}^{m} \psi_{ij}(l)$$
$$\zeta_{ij} = \sum_{l=1}^{m} \zeta_{ij}(l), \quad X_{ij} = \sum_{l=1}^{m} X_{ij}(l) \tag{61}$$

$$\chi_{ij} = Q_w(t) X_{ij} \tag{62}$$

$$\Theta_i(s) = \sum_{l=1}^{m} \Theta_i(l,s) \tag{63}$$

$$\theta_i(s) = F_s^{'}(t)\Theta_i(s) \tag{64}$$

The matrix Ξ are defined as $\Xi(t) = \Gamma^{-1} \int_{t_c}^{t} \psi(\psi+\chi)^{-1}\psi d\tau$, which can be calculated by:

$$\Xi(t) = \Gamma^{-1} \int_{t_c}^{t} \psi(\psi+\chi)^{-1}\psi d\tau = \Gamma^{-1} \int_{t_c}^{t} \psi\left(\psi + Xe^{-\omega(\tau-t_c)}\right)^{-1}\psi d\tau = \Gamma^{-1}\psi\left(\frac{\left(ln\left(E+\psi^{-1}Xe^{-\omega(t-t_c)}\right) - ln(E+\psi^{-1}X)\right)}{\omega} + (t-t_c)\right) \tag{65}$$

After getting the element expressions of Γ, ψ, ζ, χ, θ and Ξ, the matrix A can be calculated. Note that Γ, ψ and ζ are constant matrices; χ, θ and Ξ are matrices function related to time t.

The average pore water pressure $\overline{u}_{avg}(Z_l, Z_{l+1}, t)$ between depths Z_l and Z_{l+1} is given by:

$$\overline{u}_{avg}(Z_l, Z_{l+1}, t) = -\frac{\phi}{Z_{l+1}-Z_l}A(t) \tag{66}$$

where $\phi = \left[\phi_1(Z) \quad \phi_2(Z) \quad \cdots \quad \phi_N(Z)\right]$ and $\phi_j(Z) = CS\left[1, (M_j)^1\right]$.

The settlement $S(Z_l, Z_{l+1}, t)$ between depths Z_l and Z_{l+1} is given by:

$$S(Z_l, Z_{l+1}, t) = H\overline{m}_v\left(\sum_{s=1}^{K} F_s(t)\left(\frac{m_v^l \Delta Z}{2}\left(\overline{\sigma}^{l+1,s+1} + \overline{\sigma}^{l,s+1} - \overline{\sigma}^{l+1,s} - \overline{\sigma}^{l,s}\right) + \frac{\Delta m_v \Delta Z}{6}\left(\overline{2\sigma}^{l+1,s+1} + \overline{\sigma}^{l,s+1} - \overline{2\sigma}^{l+1,s} - \overline{\sigma}^{l,s}\right)\right) - \sum_{j=1}^{N} A_j(t)\left(\frac{\Delta m_v}{\Delta Z} SN\left[1,(M_j)^2\right] - m_v^l CS\left[1,(M_j)^1\right] - \Delta m_v \frac{cos\left(M_j Z_{l+1}\right)}{M_j}\right)\right) \tag{67}$$

References

Barron, R.A., 1948. Consolidation of fine-grained soils by drain wells. Trans. Am. Soc. Civil Eng. 113, 718–742.

Bergado, D.T., Anderson, L.R., Miura, N., Balasubramaniam, A.S., 1996. Soft Ground Improvement, in Lowland and Other Environments. ASCE, New York.

Bo, M.W., Arulrajah, A., Horpibulsuk, S., Chinkulkijniwat, A., Leong, M., 2016. Laboratory measurements of factors affecting discharge capacity of prefabricated vertical drain materials. Soils Found. 56 (1), 129–137.

Boyd, J.P., 2000. Chebyshev and Fourier spectral methods. Dover, New York.

Chai, J.-C., Fu, H.-T., Wang, J., Shen, S.-L., 2020. Behaviour of a PVD unit cell under vacuum pressure and a new method for consolidation analysis. Comput. Geotech. 120, 103415.

Chai, J.-C., Miura, N., 1999. Investigation of factors affecting vertical drain behavior. J. Geotech. Geoenviron. Eng. 125 (3), 216–226.

Chai, J.-C., Shen, S.-L., Miura, N., Bergado, D.T., 2001. Simple method of modeling PVD-improved subsoil. J. Geotech. Geoenviron. Eng. 127 (11), 965–972.

Deng, Y.-B., Liu, G.-B., Indraratna, B., Rujikiatkamjorn, C., Xie, K.-H., 2017. Model test and theoretical analysis for soft soil foundations improved by prefabricated vertical drains. Int. J. Geomech. 17 (1), 04016045(1–12).

Deng, Y.-B., Liu, G.-B., Lu, M.-M., Xie, K.-H., 2014. Consolidation behavior of soft deposits considering the variation of prefabricated vertical drain discharge capacity. Comput. Geotech. 62, 310–316.

Deng, Y.-B., Xie, K.-H., Lu, M.-M., 2013a. Consolidation by vertical drains when the discharge capacity varies with depth and time. Comput. Geotech. 48, 1–8.

Deng, Y.-B., Xie, K.-H., Lu, M.-M., Tao, H.-B., Liu, G.-B., 2013b. Consolidation by prefabricated vertical drains considering the time dependent well resistance. Geotext. Geomembr. 36, 20–26.

Feng, W.Q., Lalit, B., Yin, Z.Y., Yin, J.H., 2017. Long-term Non-linear creep and swelling behavior of Hong Kong marine deposits in oedometer condition. Comput. Geotech. 84, 1–15.

Hansbo, S., 1981. Consolidation of fine-grained soils by prefabricated drains. In: Proc of the 10th ICSMFE, pp. 677–682.

Hansbo, S., 2001. Consolidation equation valid for both Darcian and non-Darcian flow. Geotechnique 51 (1), 51–54.

Indraratna, B., Bamunawita, C., Khabbaz, H., 2004. Numerical modeling of vacuum preloading and field applications. Can. Geotech. J. 41, 1098–1110.

Indraratna, B., Baral, P., Rujikiatkamjorn, C., Perera, D., 2018. Class A and C predictions for Ballina trial embankment with vertical drains using standard test data from industry and large diameter test specimens. Comput. Geotech. 93, 232–246.

Indraratna, B., Nguyen, T.T., Carter, J., Rujikiatkamjorn, C., 2016. Influence of biodegradable natural fibre drains on the radial consolidation of soft soil. Comput. Geotech. 78, 171–180.

Indraratna, B., Rujikiatkamjorn, C., Sathananthan, I., 2005. Analytical and numerical solutions for a single vertical drain including the effects of vacuum preloading. Can. Geotech. J. 42, 994–1014.

Indraratna, B., Rujikiatkamjorn, C., Walker, R., 2007. Radial consolidation theories and numerical analysis of soft soil stabilisation via prefabricated vertical drains. International Workshop on Constitutive Modelling, Hong Kong, 155–167.

Kim, J.H., Cho, S.D., 2008. Pilot Scale Field Test for Natural Fiber Drain. In: In Proceedings of the 4th Asian Regional Conference on Geosynthetics, pp. 409–414.

Kim, R., Hong, S.J., Lee, M.J., Lee, W., 2011. Time dependent well resistance factor of PVD. Mar. Georesour. Geotechnol. 29 (2), 131–144.

Kim, Y.T., Nguyen, B.-P., Yun, D.-H., 2018. Analysis of consolidation behavior of PVD-improved ground considering a varied discharge capacity. Eng. Computat. 35 (3), 1183–1202.

Liu, J.-C., Lei, G.-H., Zheng, M.-X., 2014. General solutions for consolidation of multilayered soil with a vertical drain system. Geotext. Geomembr. 42 (3), 267–276.

Nguyen, B.-P., Kim, Y.-T., 2019. Radial consolidation of PVD-Installed normally consolidated soil with discharge capacity reduction using large-strain theory. Geotext. Geomembr. 47 (2), 243–254.

Nguyen, T.T., Indraratna, B., 2016. Hydraulic behaviour of parallel fibres under longitudinal flow: a numerical treatment. Can. Geotech. J. 53, 1081–1092.

Nguyen, T.T., Indraratna, B., Carter, J., 2018a. Laboratory investigation into biodegradation of jute drains with implications for field behavior. J. Geotech. Geoenviron. Eng. 144 (6), 04018026(1–15).

Nguyen, T.T., Indraratna, B., Rujikiatkamjorn, C., 2018b. A numerical approach to modelling biodegradable vertical drains. Environmental Geotechnics 1–9.

Nogami, T., Li, M., 2003. Consolidation of clay with a system of vertical and horizontal drains. J. Geotech. Geoenviron. Eng. 129 (9), 838–848.

Tang, X.-W., Onitsuka, K., 2000. Consolidation by vertical drains under time-dependent loading. Int. J. Numer. Anal. Meth. Geomech. 24 (9), 739–751.

Tang, X.-W., Onitsuka, K., 2001. Consolidation of double-layered ground with vertical drains. Int. J. Numer. Anal. Meth. Geomech. 25 (14), 1449–1465.

Tang, X., Niu, B., Cheng, G., Shen, H., 2013. Closed-form solution for consolidation of three-layer soil with a vertical drain system. Geotext. Geomembr. 36, 81–91.

Tran-Nguyen, H.-H., Edil, T., Schneider, J.A., 2010. Effect of deformation of prefabricated vertical drains on discharge capacity. Geosynthetics International 17, 431–442.

Trefethen, L. N. (2000). Spectral Methods in MATLAB. Society for Industrial and Applied Mathematics.
Walker, R., Indraratna, B., 2007. Vertical drain consolidation with overlapping smear zones. Géotechnique 57 (5), 463–467.
Walker, R., Indraratna, B., 2009. Consolidation analysis of a stratified soil with vertical and horizontal drainage using the spectral method. Géotechnique 59 (5), 439–449.
Walker, R., Indraratna, B., Sivakugan, N., 2009. Vertical and radial consolidation analysis of multilayered soil using the spectral method. J. Geotech. Geoenviron. Eng. 135 (5), 657–663.
Walker, R.T.R., Indraratna, B., 2015. Application of spectral Galerkin method for multilayer consolidation of soft soils stabilised by vertical drains or stone columns. Comput. Geotech 69, 529–539.
Wang, X.-S., Jiao, J.J., 2004. Analysis of soil consolidation by vertical drains with double porosity model. Int. J. Numer. Anal. Meth. Geomech. 28 (14), 1385–1400.
Xu, B.-H., He, N., Jiang, Y.-B., Zhou, Y.-Z., Zhan, X.-J., 2020. Experimental study on the clogging effect of dredged fill surrounding the PVD under vacuum preloading. Geotext. Geomembr. 48 (5), 614–624.
Zhou, W.-H., Lok, T.-M.-H., Zhao, L.-S., Mei, G., Li, X.-B., 2017. Analytical solutions to the axisymmetric consolidation of a multi-layer soil system under surcharge combined with vacuum preloading. Geotext. Geomembr. 45 (5), 487–498.